Observation and Simulation of Ice Tongues and Vortex Pairs in the Marginal Ice Zone

Ola M. Johannessen[1], Stein Sandven[2], W. Paul Budgell[2]
Johnny A. Johannessen[2] and Robert A. Shuchman[3]

[1] *Nansen Environmental and Remote Sensing Center / Geophysical Institute University of Bergen, Bergen, Norway.*
[2] *Nansen Environmental and Remote Sensing Center, Bergen, Norway*
[3] *Environmental Research Institute of Michigan, Ann Arbor, USA*

Investigations in the marginal ice zone of the Greenland Sea and Fram Strait have established that ice tongues can frequently propagate from the ice edge out into open water and grow into vortex pairs. The horizontal scale of these tongues and vortex pairs is typically 30 km, and the life time of the surface signature is a few days. A two-layer primitive equation ocean model is used to simulate the ice tongues and the vortex pairs in an area of 108 by 128 km with a simplified bottom topography. Ice was treated as a passive tracer and represented by particles drifting at the sea surface. No wind forcing was applied since the observed ice tongues occurred during moderate to light wind conditions. In a series of numerical experiments, where an imposed jet current along the ice edge was perturbed, ice tongues and vortex pairs similar to the observations were generated. The study demonstrates that mixed barotropic/baroclinic instability is a sufficient mechanism to generate complex mesoscale circulation and ice edge structures in the marginal ice zone. It is estimated that about 12 % of the annual ice transport past 79° N is advected out into open water by the eddies and ice tongues along the East Greenland Current.

1. INTRODUCTION

Observations as well as numerical models of marginal ice zones indicate that jets along the ice edge can occur under favorable wind conditions [*Johannessen et al.*, 1983; *Røed and O'Brien*, 1983; *Smith and Bird,* 1991; *Johannessen et al.,* 1992]. Meanders in these jets can transport ice out into open water which is readily observed in remote sensing data [*Johannessen et al.,* 1987a]. The meanders can spin off eddies which may well grow into vortex pairs which are more or less asymmetric and propagate normal to the ice edge. This phenomenon was investigated by *Fedorov and Ginsburg* [1986, 1989] who studied what they called mushroom-like currents or vortex dipoles for several years using both satellite observations and laboratory experiments. They suggested that vortex dipoles are some of the most widespread forms of non-stationary coherent motions in the ocean. Several hypotheses have been suggested to explain the generation of the ice tongues in the marginal ice zone, such as baroclinic or barotropic frontal instability, water and ice entrainment by topographic eddies, eddies within ice covered areas leading to the squirting of a jet, and ice edge upwelling. In their laboratory experiment *Flierl, Stern and Whitehead* [1983] showed that a barotropic jet emerging from a point source in a rotating fluid deflects to the right in the northern hemisphere and develops into two counter-rotating vortices. *Couder and Basdevant* [1986] studied experimentally and numerically how vortex pairs develop in two-dimensional turbulent flow. Jets and vortex pairs were also generated

The Polar Oceans and Their Role in Shaping the Global Environment
Geophysical Monograph 85

by frontal instabilities in an experiment of coastal upwelling [*Narimousa and Maxworthy*, 1987]. Numerical simulations of the generation of mushroom-like vortices by a unidirectional upper-ocean momentum patch have been conducted by *Mied at al.* [1991].

The mesoscale activity in the East Greenland Current (EGC) has been studied by several investigators during the last few years and various generating mechanisms for this activity have been suggested. *Johannessen et al.* [1987b] proposed that barotropic and baroclinic instability as well as topographic trapping are important sources for eddies. They also argued that the eddies could be advected into the EGC from the eastern part of the Fram Strait by recirculation of Atlantic Water.

In this paper the generation and decay of ice tongues and vortex pairs observed by time series of airborne Synthetic Aperture Radar (SAR) imagery combined with drifting buoys and hydrographic sections obtained in the Marginal Ice Zone Experiment of 1987 (MIZEX 87) are described. Then the results of several numerical experiments of mesoscale ocean circulation are presented, and finally, the generation of ice tongues and vortex pairs is discussed.

2. OBSERVATIONS DURING MIZEX 87

During MIZEX 87, which was located in the EGC between 76° and 79° N, mesoscale processes along the ice edge were intensively investigated during winter conditions (Figure 1). The summer experiments in 1983 and 1984 [*MIZEX Group*, 1986] had shown the importance of having SAR coverage of the same area every day in order to map the rapid changes of the ice edge processes. Therefore, a unique 12-day time series of SAR images from the Greenland Sea, combined with Seasoar and Conductivity -Temperature - Depth (CTD) sections, and data from drifting buoys, were obtained during MIZEX 87, providing detailed information of the temporal and spatial variability of ice edge features [*MIZEX Group*, 1989]. The real-time downlink of the SAR images from the aircraft to the research vessel was invaluable in the planning of buoy deployment and the CTD/Seasoar sections. Because of its high resolution and independence from light and cloud conditions, SAR is the most useful sensor for mapping of mesoscale sea ice variables such as ice edge location, detailed ice edge morphology, ice concentration, ice motion, ice types and ice edge processes [*Johannessen et al.*, 1992]. Moreover, ice floes in SAR imagery are useful tracers of upper ocean circulation if the wind conditions are moderate. During most of the MIZEX 87 experiment the winds were moderate (3 - 12 m/s) which allowed the mesoscale circulation to be mirrored by the ice floes observed by sequential SAR images.

In the X-band SAR images presented in Figure 2, 3 and 4, the sea ice of different types appear as bright signatures in contrast to open water which has a very dark signature. This is because the SAR was set for optimum ice contrast [*Johannessen et al.*, 1992]. The SAR images showed two distinct ice regimes: 1) the ice edge zone, and 2) the interior of the ice pack with large multiyear floes.

The 20 - 40 km wide ice edge zone is characterized by numerous eddies, meanders, ice tongues and vortex pairs. In this zone, the ice has a uniform and high backscatter indicating many small floes of size from 20 - 100 m. Inside the ice edge zone, large multiyear floes and clusters of such floes are seen surrounded by thin ice (dark signature). The multiyear ice clusters can be recognized from one day to

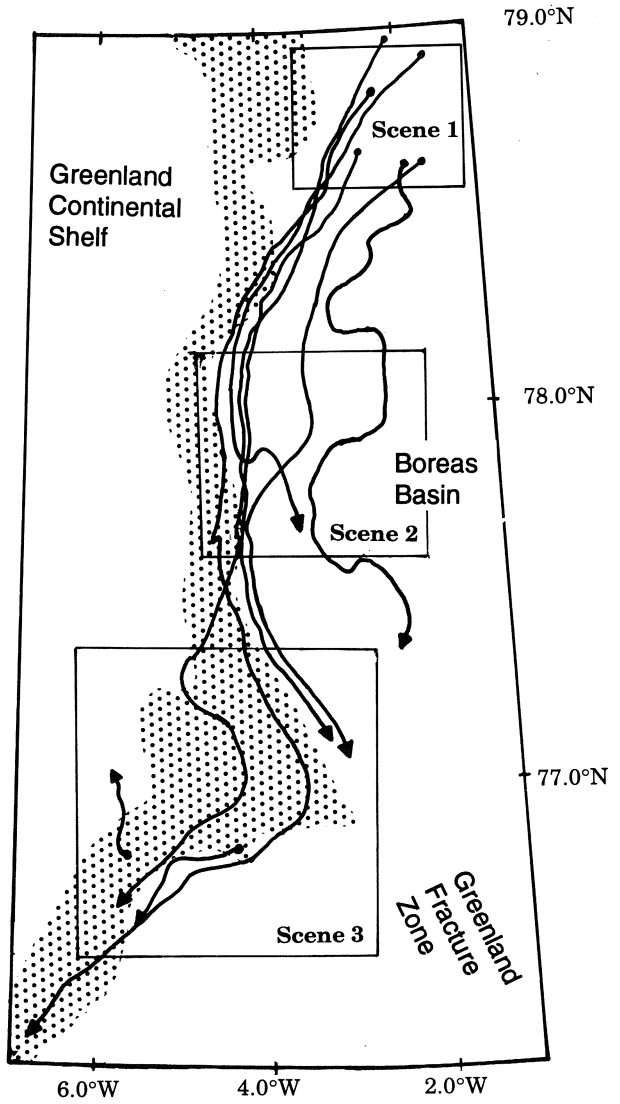

Fig.1. Trajectories of drifting buoys deployed in the ice edge region of the Greenland Sea during MIZEX 87. The shaded area indicates the continental shelf break (bottom depths from 1200 to 2000 m). The boxes mark the location of the scenes described in section 2.

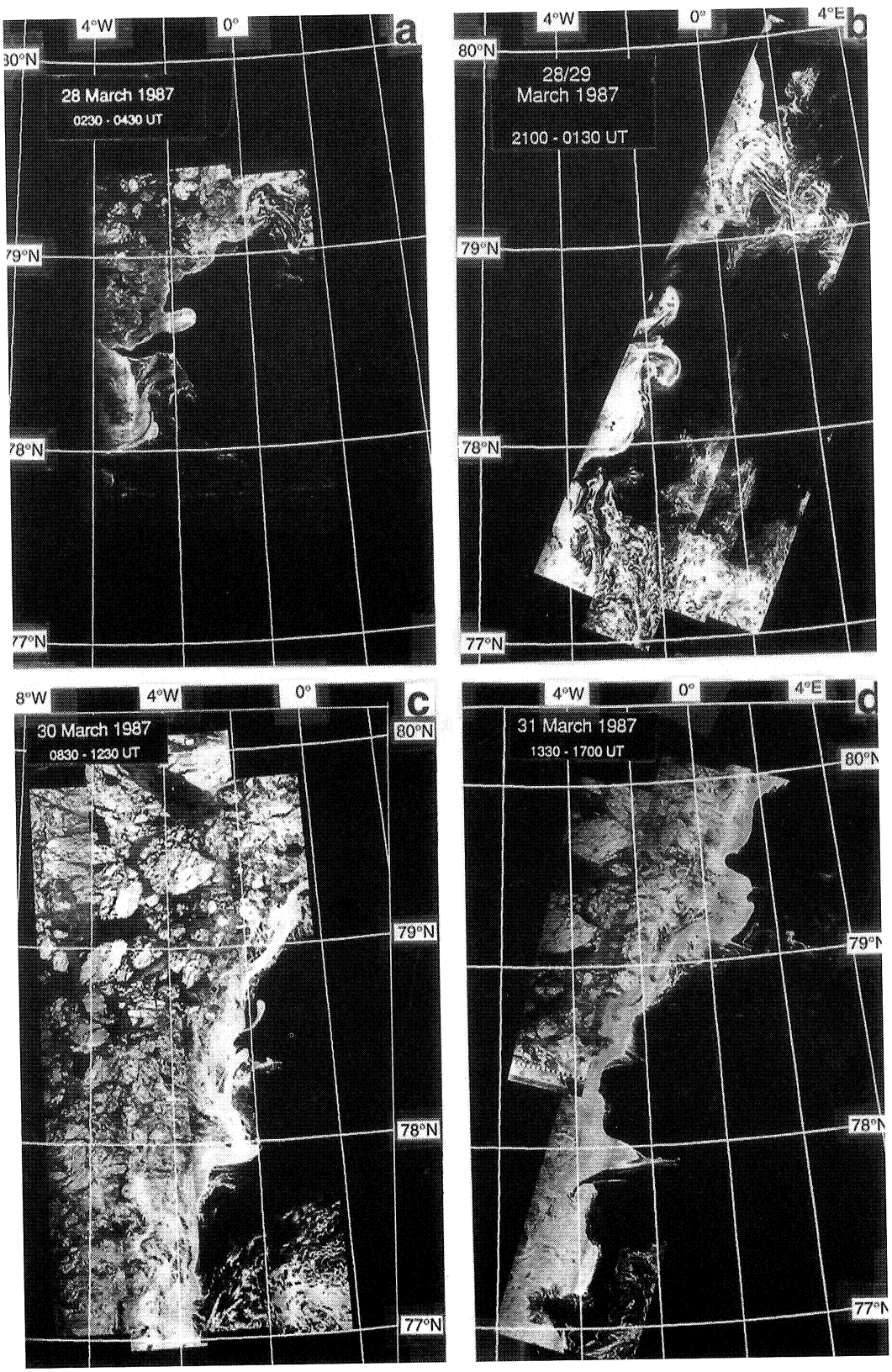

Fig. 2. Airborne X-band SAR mosaics obtained from March 28 to 31 1987.

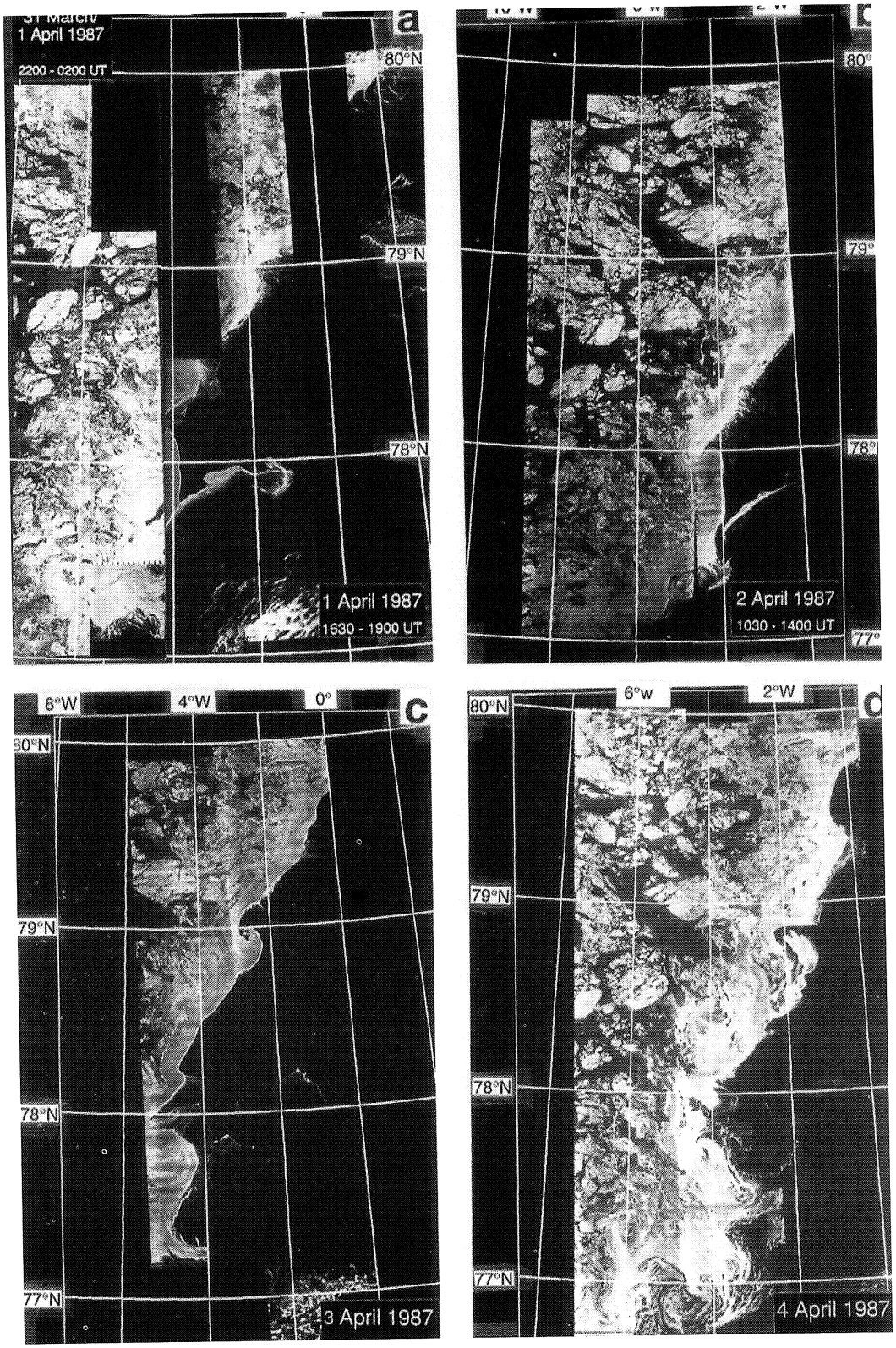

Fig. 3. Airborne X-band SAR mosaics obtained from April 1 to 4 1987.

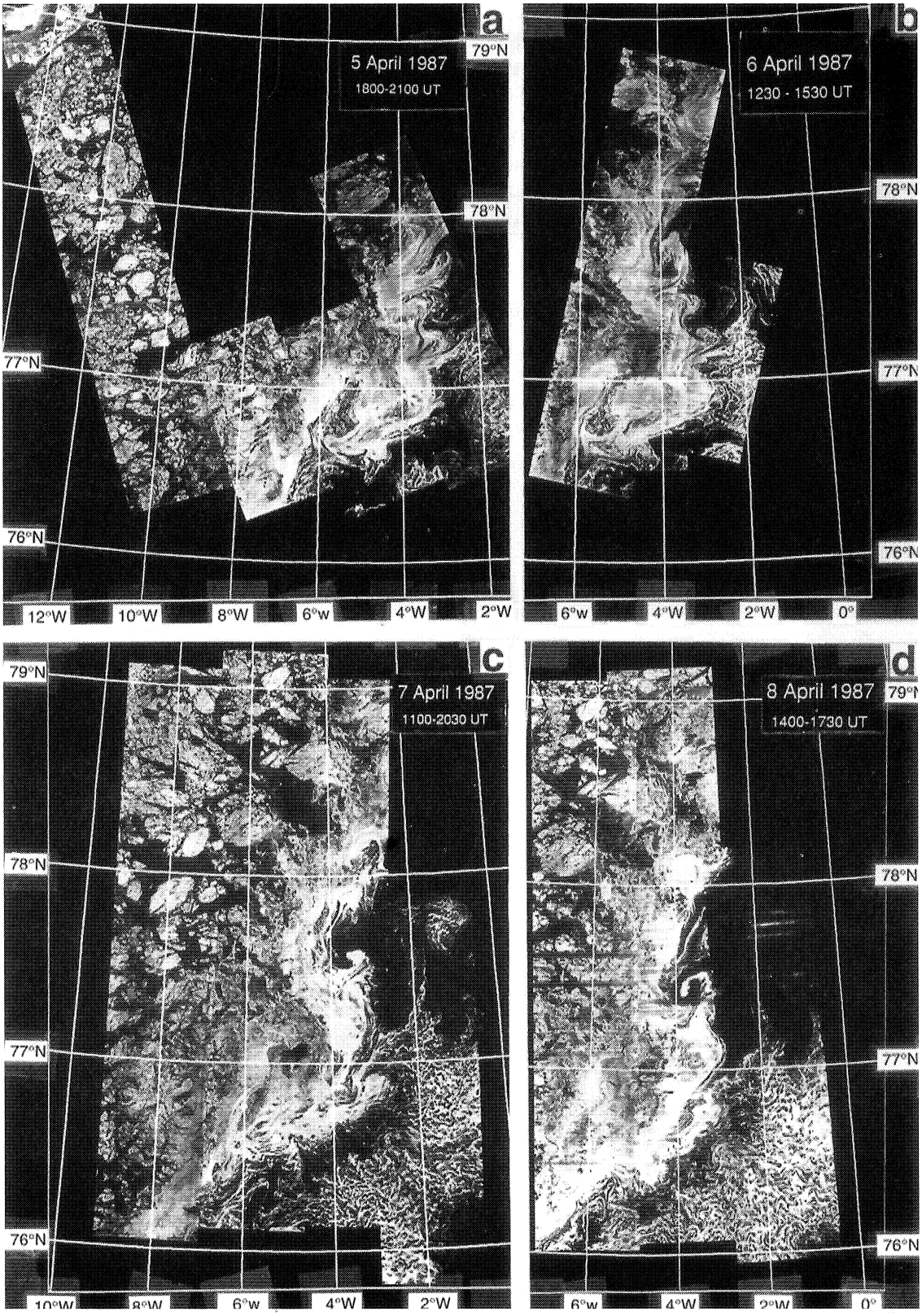

Fig. 4. Airborne X-band SAR mosaics obtained from April 5 to 8 1987.

another, thus time series of SAR images can be used to derive ice velocity vectors from the area. The sequence of SAR images display several episodes where ice eddies and tongues evolve and decay. A few of these events are selected for further examination.

An array of 10 drifting Argos buoys, three of which had current meter strings, were deployed in the ice edge region, providing ice and ocean velocity at various depths down to 250 m (Figure 1 and 5). Zonal velocity profiles across the ECG were obtained from the array, while the current meter strings provided vertical velocity profiles.

2.1. *Scene 1: Ice tongues and vortex-pair north of 78°30' N.*

In the period from March 28 to 31, the growth and decay of two ice tongues were observed in a sequence of four SAR images (Figure 6) and documented by CTD and Seasoar sections. The image obtained early in the morning on March 28 showed two tongues of ice shooting out from the ice edge. The northern tongue was characterized by a compact and well-defined ice edge. Later in the morning, as the icegoing vessel "Polar Circle" obtained a CTD section along 78° 50'N, the northern tongue was also observed from helicopter. The southern tongue which had the signature of an anticyclonic eddy was more diffuse with lower ice concentration, but the SAR image showed clear ice bands extending out into the open ocean. The wind was 5 m/s decreasing to 2 m/s from northeast during the day.

One day later the northern tongue had developed into a well-defined mushroom-shaped vortex-pair with horizontal scale of about 20 km (Figure 6 b). The front of the tongue did not show any eastward or southward advection. Approximately 8 hours after the SAR acquisition time a helicopter survey of the northern ice tongue showed that it was growing into a cyclone. Meanwhile, the southern tongue turned into an anticyclone about 30 km in diameter.

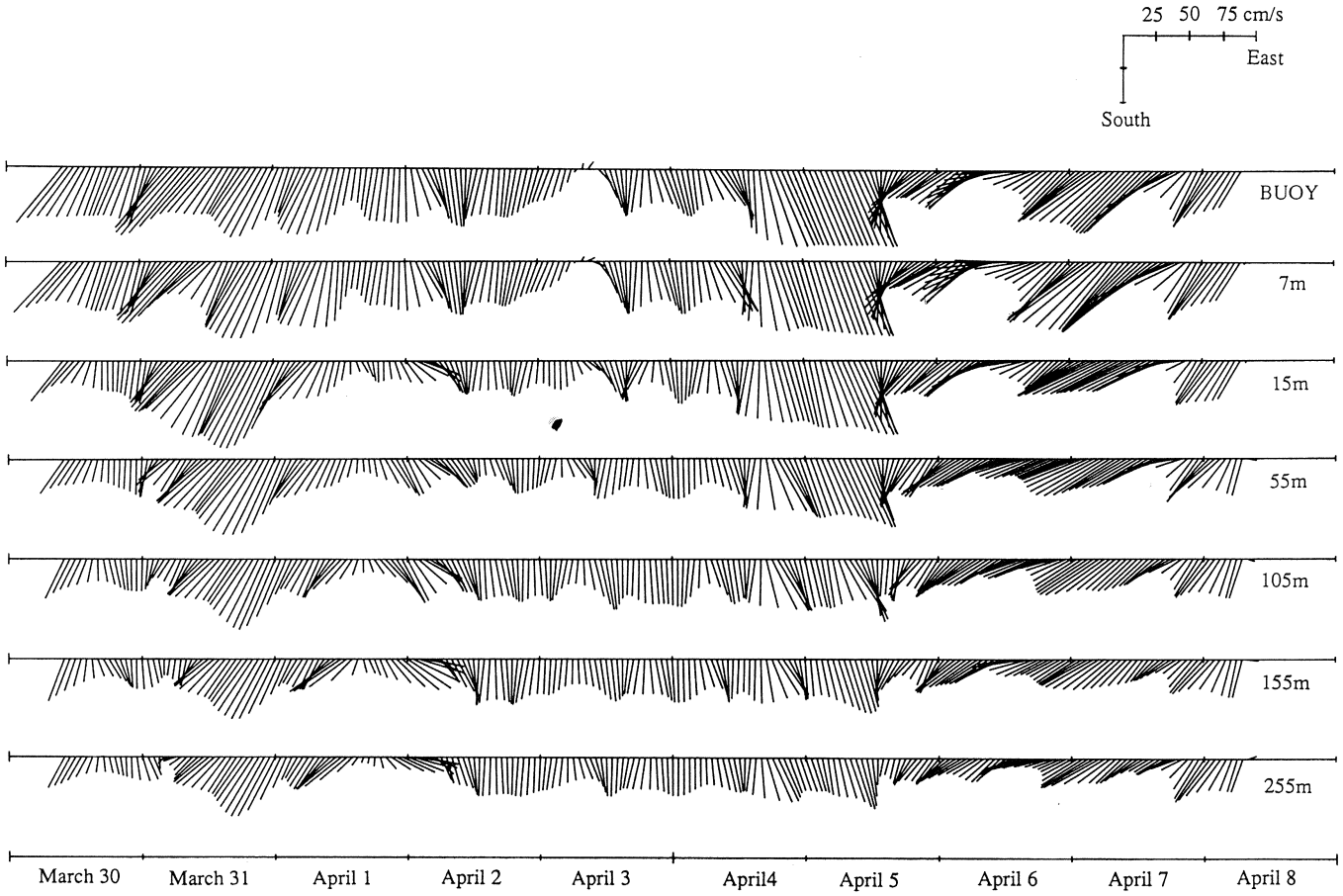

Fig. 5. Time series of ice and ocean velocity vectors at different depths from buoy 5064 with suspended current meters. The ice velocity is calculated from Argos positions interpolated to hourly values. The absolute ocean velocity is estimated by adding relative ocean velocity to the ice velocity. All vectors are plotted every hour and high frequency noise (cutoff period of 3 hour) has beeen removed from the data.

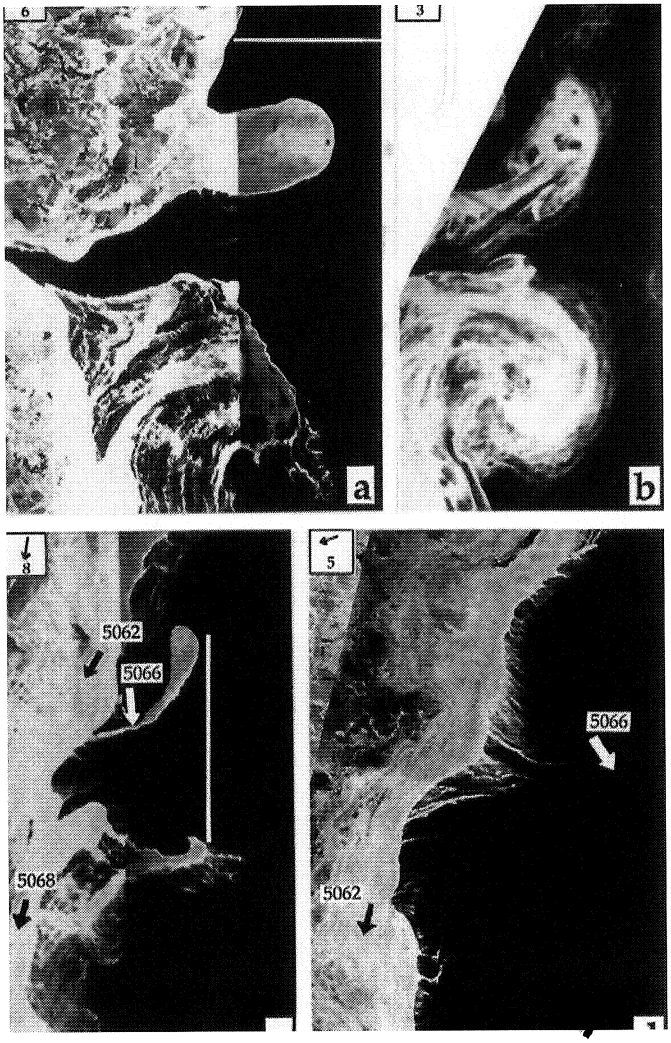

Fig. 6. Zoomed SAR images of the scene 1 area showing growth and decay of two ice tongues and a vortex pair between 78° and 79° N. The images were obtained on (a) March 28 0300 Z, (b) March 29 0100 Z; (c) March 30 1100 Z and (d) March 31 1400 Z. White/grey is ice while black is open water. White lines in (a) and (c) mark the location of CTD and Seasoar sections. At the time of each SAR image the buoy drift is indicated by bold arrows and the wind (m/s) is inserted in the upper left corner.

On March 29 several Argos buoys were deployed in the ice edge region. Buoy (5066) was dropped in open water to the north of the cyclonic center, while another (5068) was deployed on a floe south of the cyclone´s center (Figure 7). The trajectory of 5066 indicated that it was caught in the cyclonic eddy; first it drifted westwards and then towards south along the main ice edge, before it turned southeastward into open ocean. Buoy 5068 drifted towards southwest and into the main ice pack. A third buoy, 5062, deployed north of the eddy, remained inside the ice edge throughout the experiment. The Argos buoys and the SAR images showed that the core of the EGC as well as the mean ice edge was located along the slope of the continental shelf.

The zonal velocity profile (from the Argos buoys) across the EGC had a maximum of 0.40 - 0.60 m/s at the ice edge and decreased to about 0.20 m/s further into the ice. In the open ocean the velocity field was dominated by eddies and the mean southward current was weaker (below 0.10 m/s).

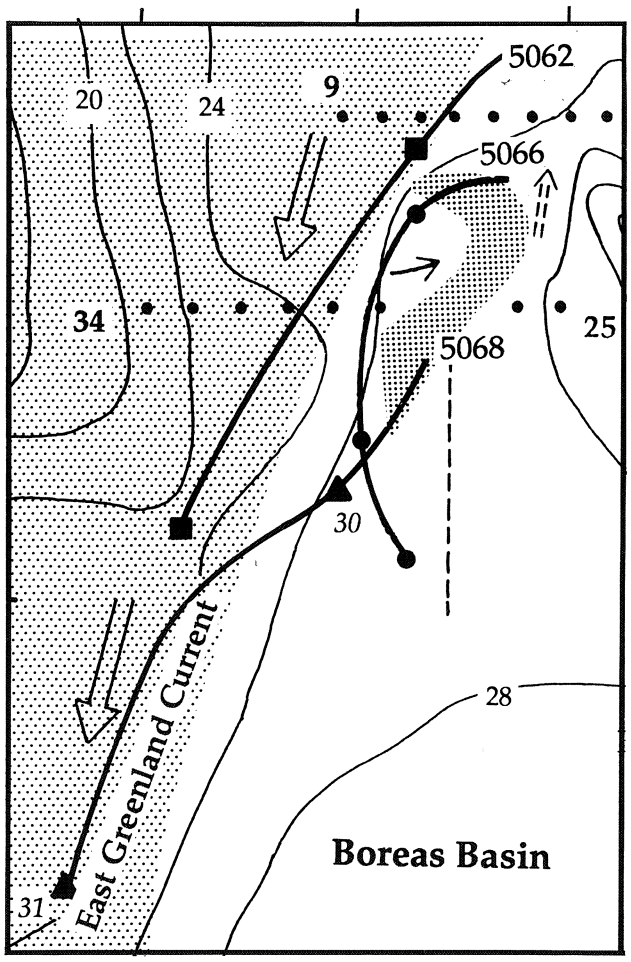

Fig. 7. Bathymetric chart of scene 1 area, the northern Boreas Basin including the East Greenland Current (bold arrows) and the mean ice-covered area (shaded area). The shape of the cyclonic ice tongue (shaded area off the ice edge) was observed from helicopter 8 hours after the image in Fig. 6 b. Small dots indicate two deep CTD sections oriented in east-west direction, and the dashed line mark the north-south Seasoar section. The vertical temperature structure in these sections are shown in Fig. 8. Bold lines are the trajectories of buoys 5062, 5066 and 5068 from March 29 to 31. A northerly current (dashed bold arrow) east of the ice tongue is derived from geostrophic calculations of the CTD sections. Bottom contours are in hectometer.

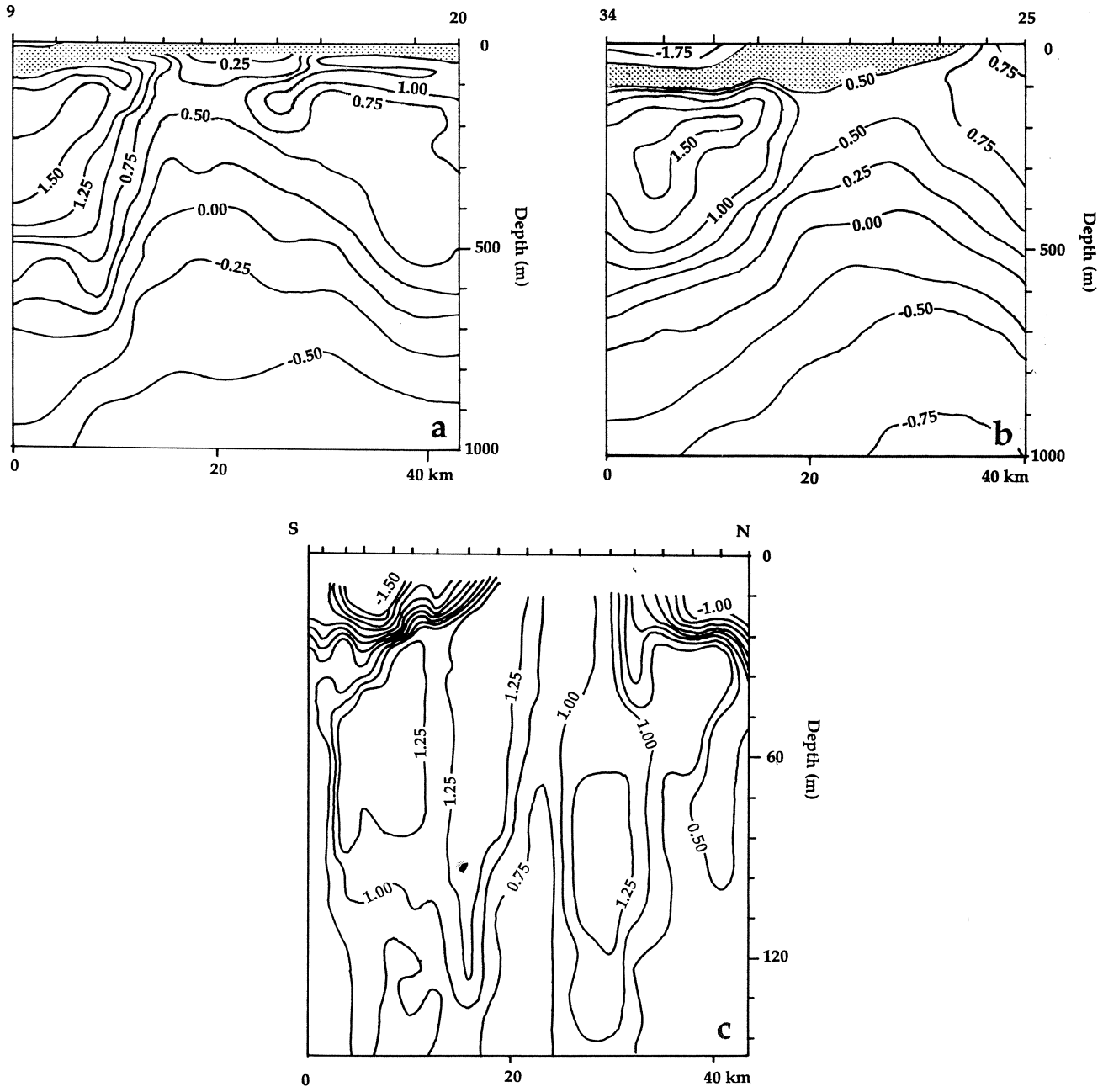

Fig. 8. Vertical sections of temperature obtained by the "Polar Circle" on (a) March 28 and (b) 31, respectively. The thermocline (from -1.5° to 0.5° C) is shaded. The Seasoar temperature section (c) was obtained by the "Håkon Mosby" on March 30 across the front of two ice tongues. Station spacing is approximately 2 km. The location of the three sections is shown in Fig. 7.

On March 30, the third SAR image (Figure 6 c) showed that the vortex pair had been reduced to a smaller tongue of ice which was oriented towards the north. The surface signature of the cyclone, which was clearly seen the previous day, was about to collapse due to an increasing northeasterly wind of 10 - 12 m/s. Also, the anticyclonic tongue was diminishing. The fourth SAR image obtained on March 31 showed no sign of any ice tongues. After a period of easterly winds 6 - 12 m/s the remnants of the tongues had been pushed back into the main ice edge,

indicating that the wind was the dominant ice forcing mechanism on this day, thus masking the ocean circulation. Melting could also play a role to diminish the ice tongue.

Based on the real-time SAR images downlinked to the "Polar Circle" a CTD section was obtained across the ice edge (Figure 7 and 8 a), while the northern ice tongue developed into a vortex-pair. The EGC is seen in the western part of the section as a sloping boundary separating the relatively cold and fresh surface water from the warmer and more saline Atlantic Water between 50 and 300 m. In the center of the section deep water masses dome towards the surface surrounded by Atlantic water. In the western part of the section the southerly geostrophic velocity relative to 1000 m is up to 0.20 m/s, while it is 0.05 - 0.10 m/s to the north in the eastern part. These observations confirm the presence of a cyclonic eddy with a diameter of 30 - 40 km extending at least down to 1000 m. A second east-west CTD section, 15 km to the south, was obtained by the "Polar Circle" three days later, on March 31, (Figure 8 b) and showed the same characteristics as the first section. The trajectory of buoy 5066, shown in Figure 7, also indicated the cyclonic circulation.

On March 30 the research vessel "Håkon Mosby" obtained a Seasoar section in front of both the ice tongues while they were in the decaying phase. This section showed that the ice tongues were associated with a 20 m thick surface layer of cold Polar Water on top of a core of Atlantic Water between 30 and 120 m (Figure 8 c). This water mass structure is characteristic for the core of the EGC. As this water propagates to the east the surface layer becomes shallower and the isotherms rise to the surface.

2.2. *Scene 2: Ice tongue and vortex-pair at 78° 00' N*

The second occurence of ice tongues was observed from March 30 to April 2. The growth of this tongue is illustrated schematically in a composite of the ice edge from four SAR images (Figure 9). The tongue started on March 30 as a meander of the main ice edge at 78°00' N. The day after a well-defined tongue had formed and moved about 10 km towards the east. In the following two days the tongue was advected southwards and changed its orientation due to the zonal velocity shear across the EGC. In spite of an on-ice wind of up to 12 m/s the tongue grew eastwards and retained its structure. Examination of the 31 March SAR image (Figure 10 a) clearly shows an ice distribution that traces the velocity structure within the tongue.

One of the Argos buoys (5068) was drifting in the tongue, providing quantitative information on the ice velocity. As the buoy approached the center of the tongue on its northern side it drifted east-southeast at 0.30 - 0.40 m/s. Instead of being advected further east and out into open water it suddenly turned southwest and increased its speed to 0.70 - 0.80 m/s in the southern part of the tongue (Figure 11). During the next day the tongue was stretched

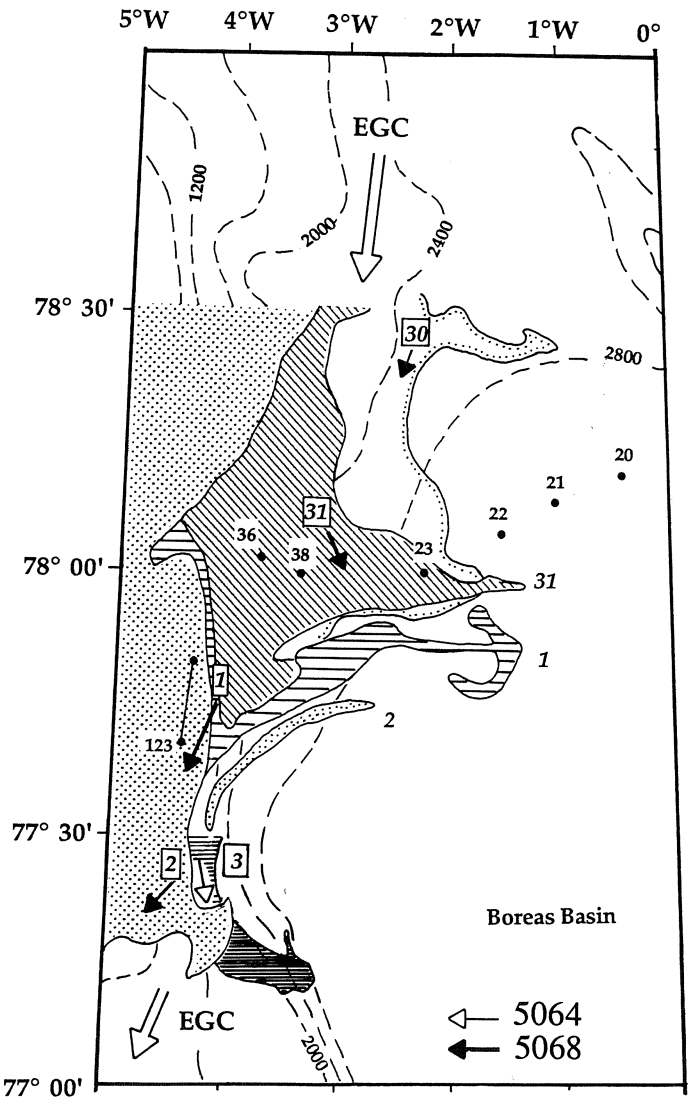

Fig. 9. Composite map of ice edge from daily SAR images between March 30 and April 3 superimposed on a bathymetric chart. Dates are shown in italics and black dots indicate CTD stations. Thin arrows mark position and drift velocity of ice buoys at the time of the SAR images. Bold arrows indicate the core of the East Greenland Current (EGC).

as it was advected southwards. In front of the tongue a vortex pair was formed with a horizontal scale of 20 km (Figure 10 b). Both the cyclonic and anticyclonic parts of the vortex pair were clearly developed. One day later the surface signature of the vortex pair had vanished. The life-time of the tongue is estimated to be 2 - 3 days and the length was up to 50 km. The two ships attempted to characterize the subsurface structure of the water below the ice tongue but did not succeed due to the rapid growth and decay of the tongue.

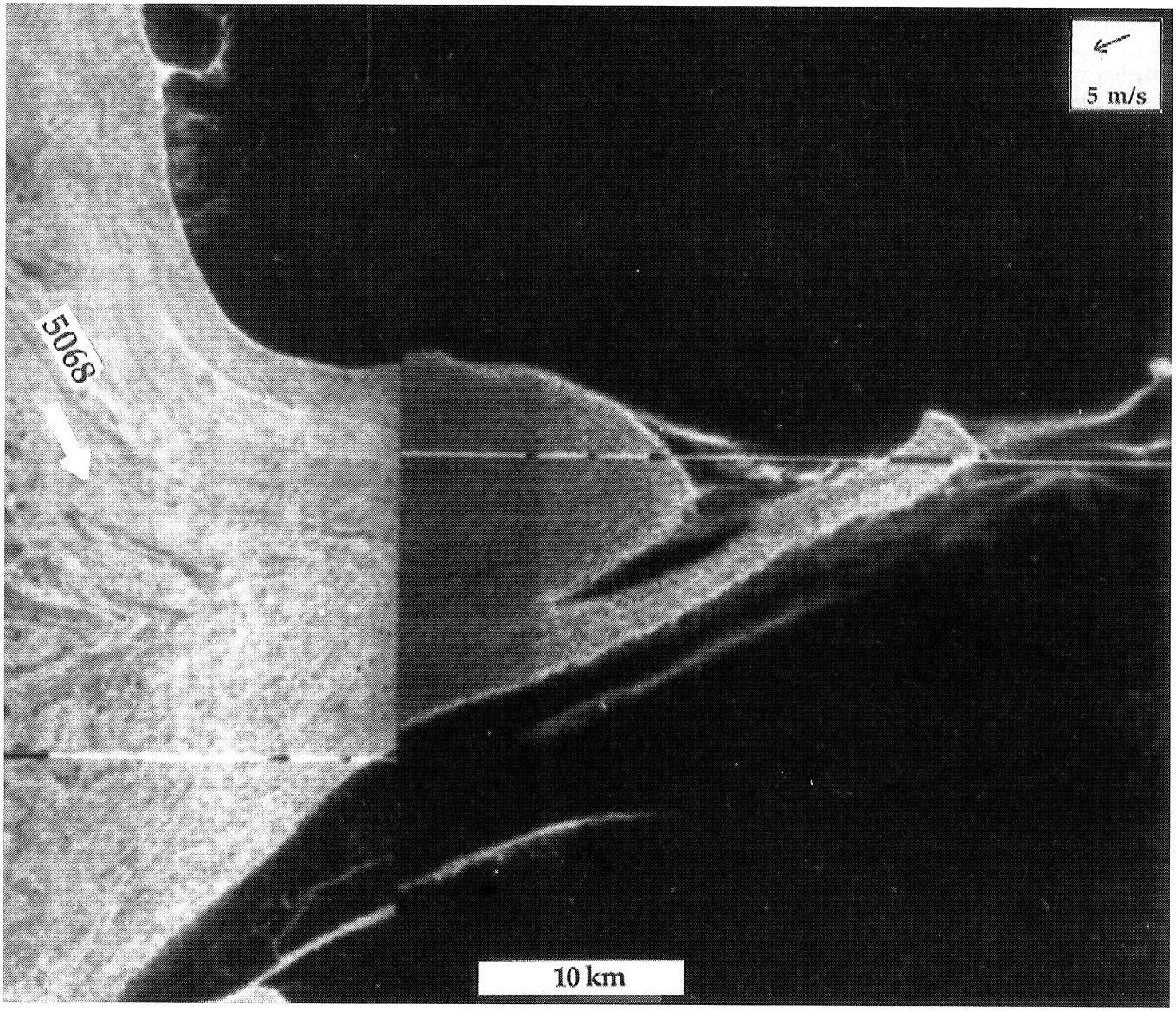

Fig. 10. (a) A zoomed SAR image with resolution of 15 m obtained on March 31 at 78° 00' N where a tongue of ice is evolving. The bold white arrow indicates drift of buoy 5068. (b) SAR image from the same area obtained one day later (April 1). The isecond mage shows how the tongue is stretched and the development of a vortex-pair.

2.3. *Scene 3: Southerly jet and anticyclonic eddy.*

In the SAR image of April 2, a fan-shaped ice tongue is seen to develop in a southeasterly direction normal to the ice edge at 77° 20' N 4° W (Figure 12 a). The tongue is seen as scattered ice advected out from the main ice edge. The wind was northerly 6 m/s. During the next day, when the wind was 8 m/s from northwest, a well-developed tongue of more compact ice was formed and advected out from the main ice edge in a southeasterly direction (Figure 12 b). The SAR image also shows filaments of ice which extend out from the ice tongue as well as stripes of lower concentration inside the tongue, having the form of a vortex pair at the other end of the tongue. The width of the main tongue is about 10 km and the length is approximately 20 - 25 km at the time when the SAR image was obtained. In contrast to the tongues in scene 1 and 2, which propagated against the wind, this jet developed in the same direction as the wind. The front of the tongue was advected about 20 km in one day to the southeast (Figure 9).

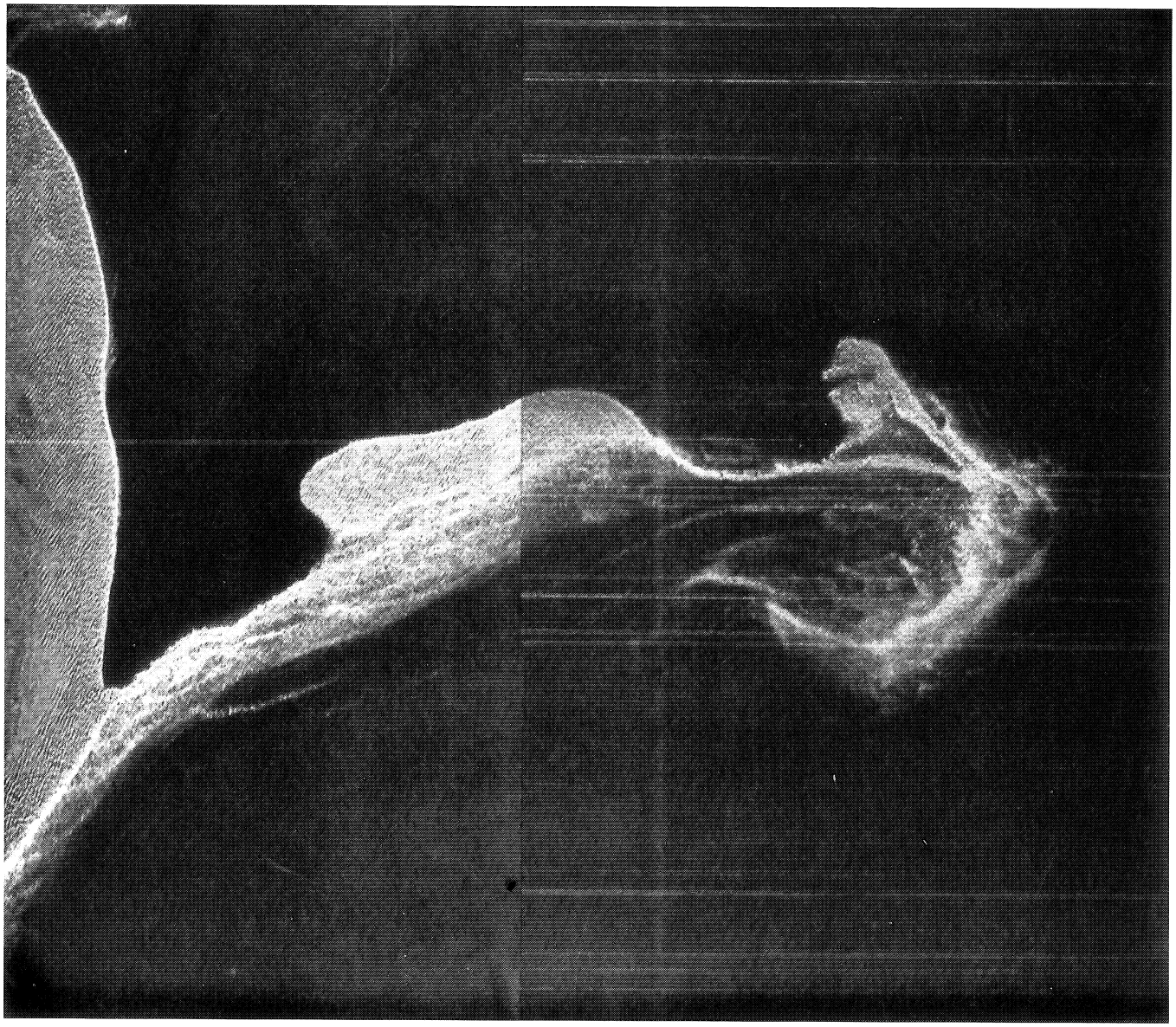

Figure 10. (continued)

The drifting buoys showed that this tongue was associated with a strong oceanic jet parallel to the isobaths. On April 4 the easternmost buoys (5064 was one of them) were caught by the jet and advected southeastward out into open water and had to be recovered in the afternoon (Figure 13). Buoy 5063, which was initially located only two miles further into the ice compared to 5064, was initially caught in the jet but was detached from it towards the end of the day. Buoy 5068 was located 10 - 15 km into the ice pack and drifted southwards at a slower speed, about 0.20 m/s. The surface speed of the jet, as measured by the drift velocity of 5064, exceeded 1.0 m/s and the horizontal shear between 5064 and 5063 was as strong as 10^{-4} s^{-1}, on the same order as the Coriolis parameter.

Mean vertical profiles of velocity and temperature of the jet as well as the core of the EGC, estimated for April 4, are shown in Figure 14. The velocity profile of buoy 5063, which followed the core of the EGC, had a maximum of 0.60 m/s at the surface and decreased to about 0.30 m/s at 250 m. The jet, which branched off towards the southeast along the isobaths, had a similar profile but with 0.30 - 0.40 m/s higher values in the upper 250 m of the water column. The temperature profiles were similar at the two buoys, with cold polar water in the surface layer and warmer

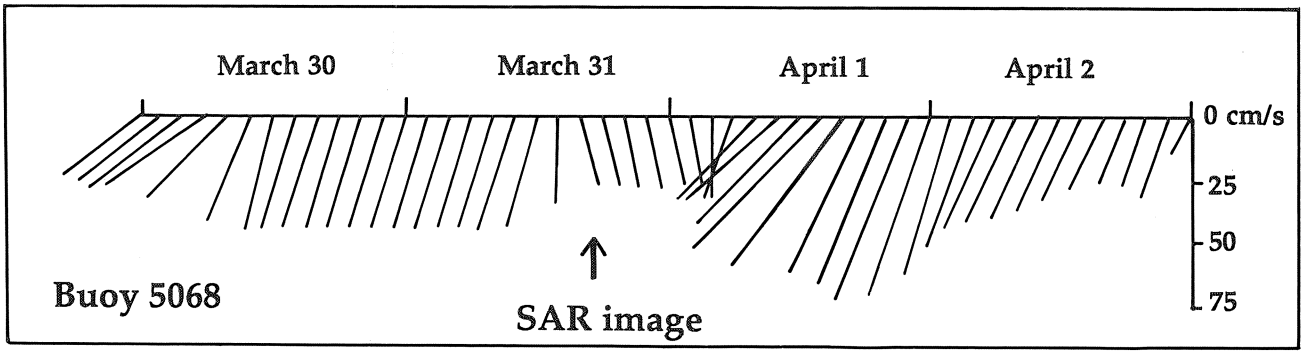

Fig. 11. Velocity vectors of buoy 5068 from March 30 to April 2.

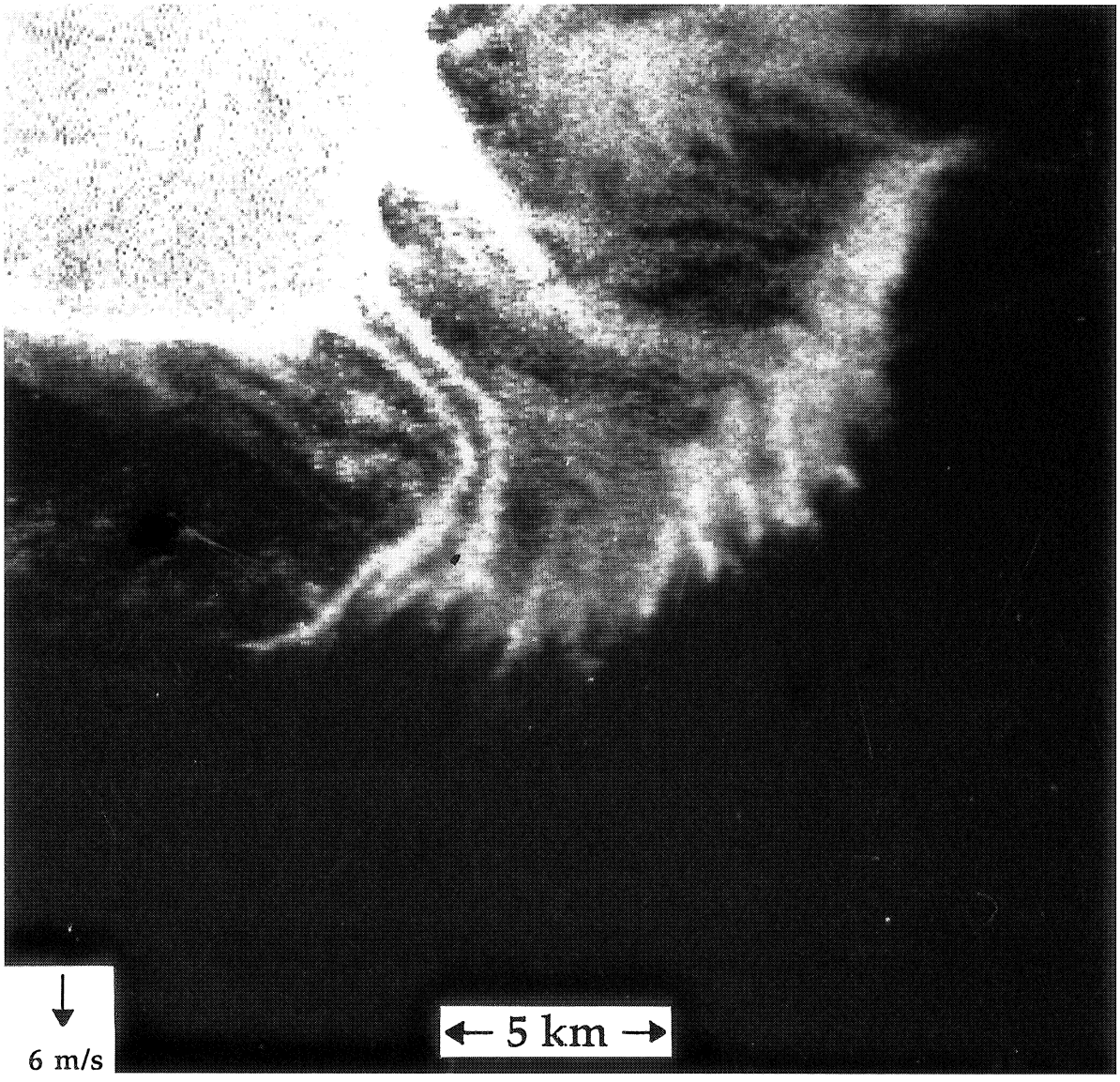

Fig. 12. SAR images showing the evolution of a south-easterly ice tongue on (a) April 2 and (b) April 3. The location of the tongue is shown in Fig. 9 at about 77° 15' N.

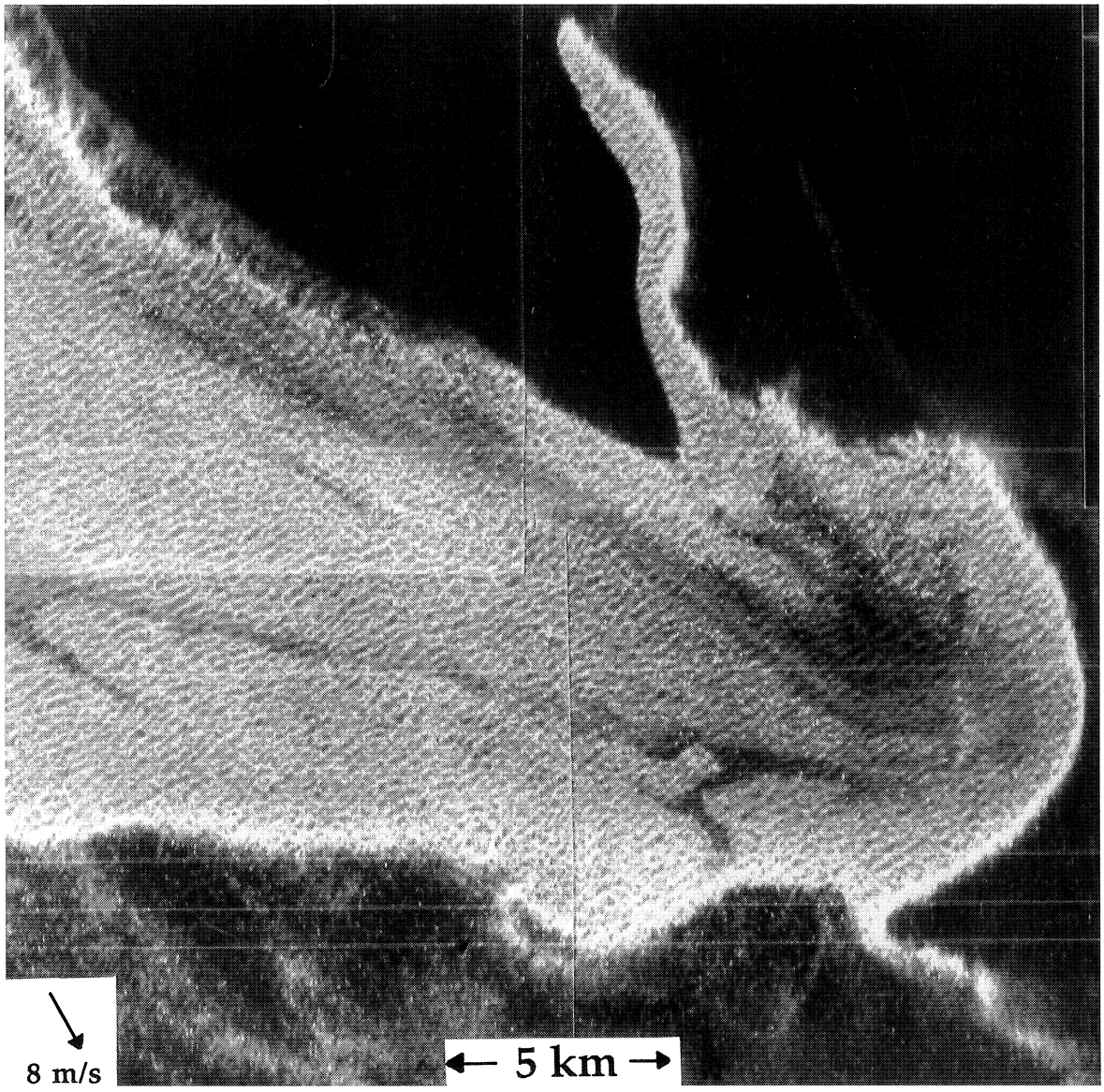

Figure 12. (continued)

Atlantic Water below 150 m. Characteristic density profiles from CTD data are used to estimate a stratification parameter to be used in the two-layer model described in section 3. Upper and lower layer density of 1027.2 kgm^{-3} and 1027.9 kgm^{-3}, respectively, yield a reduced gravity $g' = 0.007\ ms^{-2}$. Similarly, upper and lower layer velocity values to be used in the model were obtained from the current meter data.

In contrast to the upper layer short-lived ice tongues described in scene 1 and 2, this jet penetrated deeper than 250 m (Figure 14) and propagated along the isobaths which are directed to the southeast in this area because of the Greenland Fracture Zone. A likely explanation is that this topographic feature can branch off a part of the EGC which is entrained in gyre scale cyclonic circulation outside the ice edge in the Boreas Basin [*Quadfasel and Meincke*, 1987; *MIZEX Group*, 1989]. The observed jet could therefore be an indication of this circulation along the pronounced bottom topography of Greenland Fracture Zone.

On April 4 the ice jets had developed into a large anticyclonic eddy near the Greenland Fracture Zone at 77° N (Figure 13). As the array of buoys drifted through the anticyclone they documented the velocity of the ice as well as the upper ocean current. The ice and upper ocean velocity was 0.50 m/s, decreasing to about 0.30 m/s at 250

Fig. 13. The displacement of three buoys (5068 west, 5063 center, and 5064 east) from April 3 1800 Z to April 4 1800 Z superimposed on the SAR image of April 4. The length of the velocity vector of 5064 is 50 km.

m. A composite of SAR ice edge positions between April 4 and 6 combined with ice velocity vectors from the buoys shows the surface characteristics of the anticyclone (Figure 15). A deep CTD section was successfully obtained through the center of the eddy by using real time SAR images (Figure 16). The section documented the anticyclonic rotation by a characteristic downward doming of the isopycnals in the eddy center. In addition to the surface ice transport, a dominant feature was a core of Atlantic water circulating at a radius of 20 km from the eddy center at a depth between 200 and 400 m. The geostrophic velocity estimates showed that the southward flow in the upper 100 m was above 0.40 m/s, in good agreement with the buoy velocities. From this eddy, which had a diameter of about 50 km, several smaller jets and vortex-pairs were pinched off (Figure 4 a, b). The interaction of the EGC with the abrupt topographic change at 77° N is a probable generating mechanism for this anticyclone.

2.4. *Other observations*

The spatial distribution of ice tongues over a larger area was analyzed using an AVHRR satellite image of July 1 1984. The image shows a cloudfree ice edge from about 75° to 79° N with at least eight ice tongues or eddy features (Plate 1). The ice tongue at about 78° (# 3) is remarkable

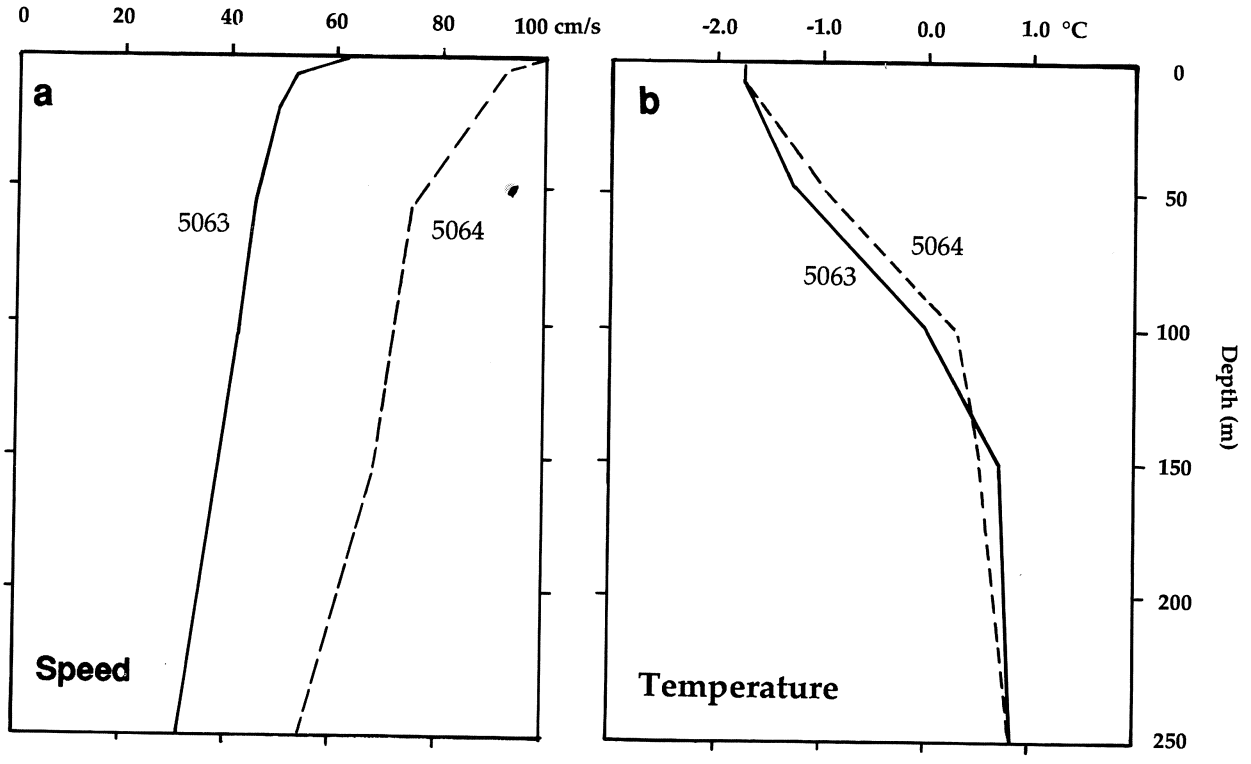

Fig. 14. (a) Vertical velocity profile of 5063 (outside the jet) and 5064 (inside the jet) on April 4. (b) Vertical profile of temperature from the same buoys.

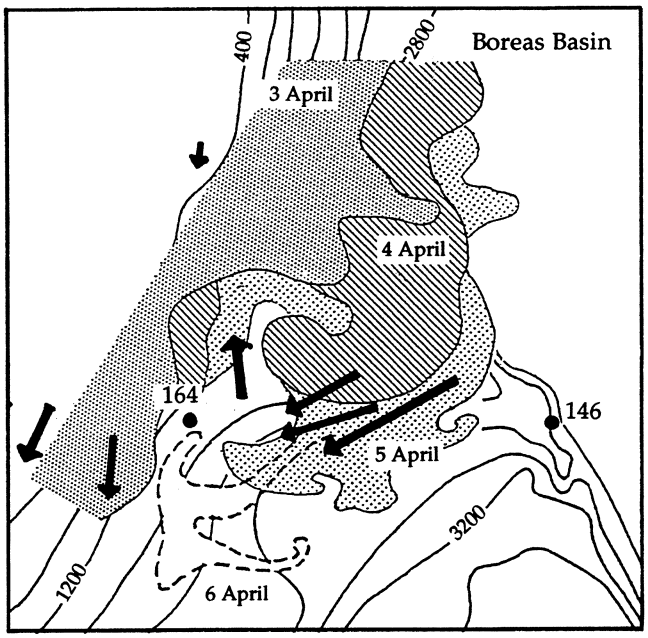

Fig. 15. A composite of the ice edge obtained from daily SAR images between April 3 and 6 superimposed on the bottom topography. Included are also ice velocity vectors from drifting buoys (bold arrows). The two bold dots (146 and 164) mark the end points of the CTD section taken across the anticyclone.

similar to Figure 10 a. At 76° 30' N a tongue of cold water and ice (# 5) is advected to the east, probably caused by the topography, which was disussed in section 2.3. Further south two tongues of ice (# 6 and 7) grow out in open water and develop into vortex pairs. The horizontal scale of all these eddy features is 30 - 50 km, similar to the observations in 1987. The image also shows a characteristic separation between each ice tongue of 50 km.

In January 1992 SAR images from the ERS-1 satellite were obtained during another field experiment by the "Håkon Mosby" in the same area as MIZEX 87. These SAR images covered 600 km long and 100 km wide swaths in the ice edge region between 75° and 80° N (Plate 2, a). On January 13 an anticyclone was observed in same location as in MIZEX 87 (77° N 4° W). The anticyclone had a vortex-pair directed in a southwesterly direction. In addition the ERS-1 SAR image showed several tongues of ice extending out from the main ice edge. Since the ERS-1 had a repeat cycle of three days, daily mapping of the growth and decay of the tongues could not be obtained. However, a 300 km long Seasoar section, measuring ocean temperature, salinity and density in the upper 100 m was taken parallel to the ice edge (Plate 2 b, c, and d). This section ran across several cold plumes of water associated with tongues of ice extending out from the ice edge. The section showed a complex horizontal structure with typical scales of 10 km or less. The plumes of cold low salinity water associated with the ice tongues were deeper than 100 m. The data from 1992 confirm several of the features observed in the MIZEX 87 experiment, demonstrating that eddies, ice tongues and vortex-pairs occur frequently in the area and that the anticyclone at 77° N may be a more permanent feature.

2.5. Summary of observations

The interpretation of the ice velocity field from SAR or other images (AVHRR) is not a straightforward procedure. The problem is to separate the Lagrangian from the Eulerian description of the velocity field. Therefore, ice features seen in the SAR images cannot be used to estimate velocities directly. Another problem is that the ice may not be a passive tracer which drifts freely. It can have its own dynamics, in contrast to the filaments off California and dyed streamers in tank experiments. With this in mind the observations of eddy features in the marginal ice zone of the Greenland Sea can be analyzed.

A typical length scale of the ice tongues and vortex pairs along the ice edge is 30 km. The lifetime is more difficult to estimate, but the ice signature from a time series of SAR images combined with CTD data suggests that in the upper structure (< 30 m depth) it can be as short as 3 - 4 days, while the deeper structures last much longer (> 10 days). The SAR images showed several cases where a filament of ice shoots off the ice edge one day and grows into a fully developed vortex pair the next day. One or two days later it has degenerated. This apparent degeneration may be due to ice which diffuses and melts or ice advection by the wind. Thus the surface ice signature may disappear and obscure the subsurface structure of the circulation which can persist for a longer period. In situ data from the ships and the drifting buoys were therefore of vital importance to supplement the SAR data in the interpretation of the circulation.

The background circulation for the ice tongues and vortex pair observations described in this paper is a boundary current flowing along a continental shelf break as well as a front separating colder and fresher Polar Water from warmer and more saline water masses of Atlantic origin. In addition, there is an ice edge separating open water from pack ice which has its own dynamics. Boundary currents and frontal jets, as described in section 2.3, are deeper and more permanent than the ice tongues extending out from the ice edge. These tongues or filaments, often with a vortex-pair in the front, are shallow (30 - 100 m) and have a lifetime of a few days. It is hypothesized that local dynamic instability of synoptic scale motions such as meanders, eddies and frontal jets plays an important role in their formation.

3. NUMERICAL MODEL

In this section, a model for describing the generation of ice eddies, tongues and vortex pairs through mixed

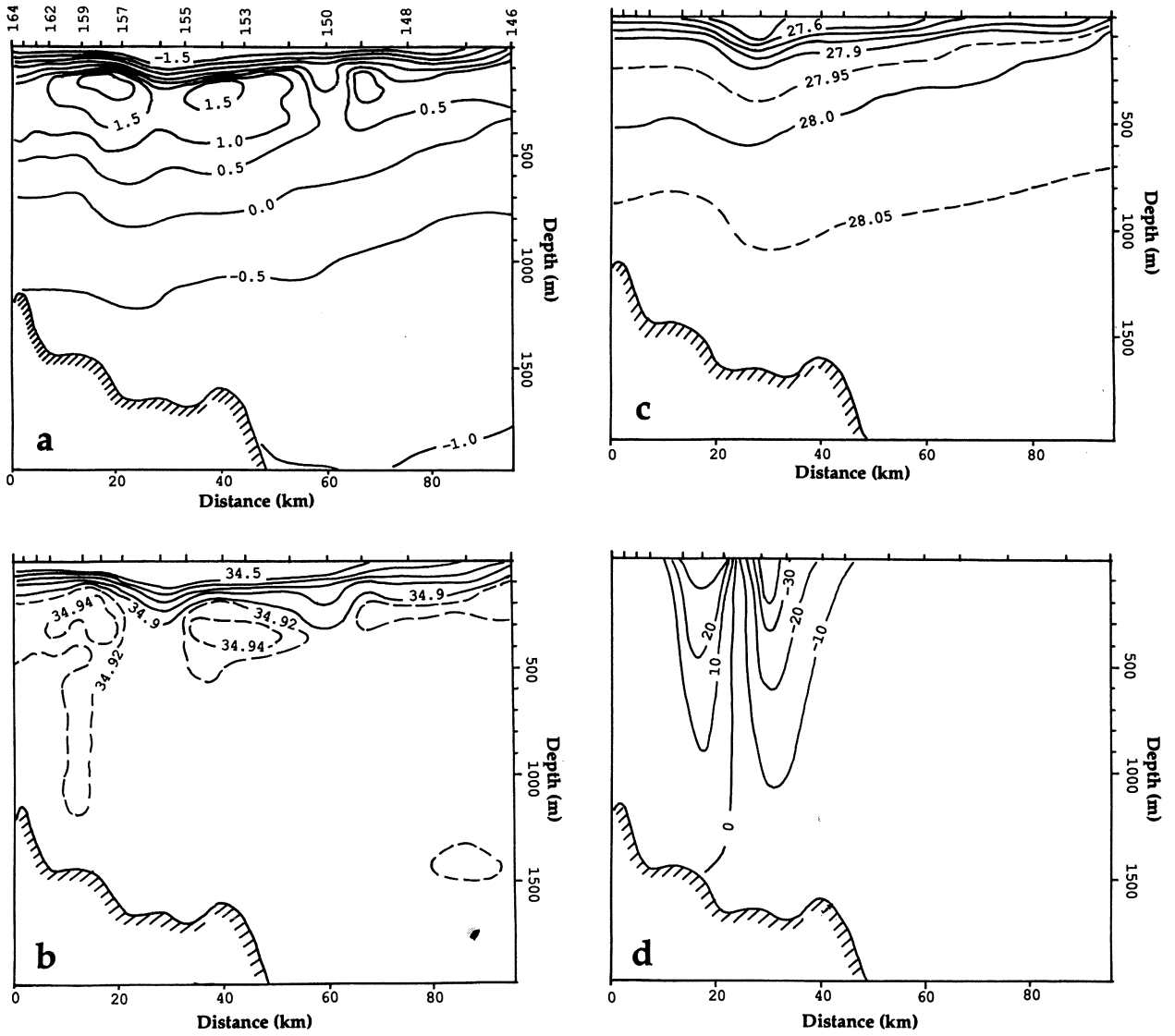

Fig. 16. CTD section across the anticyclone: (a) potential temperature, (b) salinity, (c) potential density, and (d) geostrophic velocity.

barotropic-baroclinic instability is defined. In the study, a two-layer primitive equation representation of the ocean is employed with typical parameters derived from the MIZEX 87 experiment.

3.1. Governing Equations

The governing equations for the model consist of statements of momentum and mass conservation for a two-layer ocean:

$$\frac{\partial \mathbf{V}_i}{\partial t} + \left(\nabla \cdot \mathbf{V}_i + \mathbf{V}_i \cdot \nabla\right)\mathbf{v}_i + f \times \mathbf{V}_i = -h_i \nabla P_i - A_{bh} \nabla^4 \mathbf{V}_i \quad (1)$$

$$\frac{\partial h_i}{\partial t} + \nabla \cdot \mathbf{V}_i = 0 \quad (2)$$

The symbols are defined in Table 1. Sea ice is treated as a passive tracer in this study, and is represented by Lagrangian particles drifting on top of the ocean surface. This means that no ice dynamics are used implying that wind forcing as well as internal ice stress are absent. The only mechanism for ice motion is the surface velocity of the ocean. The neglect of wind forcing is normally not realistic, but can be justfied in these experiments because the wind conditions during the field experiment were moderate and most of the mesoscale activity was caused by the ocean dynamics. The neglect of internal ice stress is assumed to

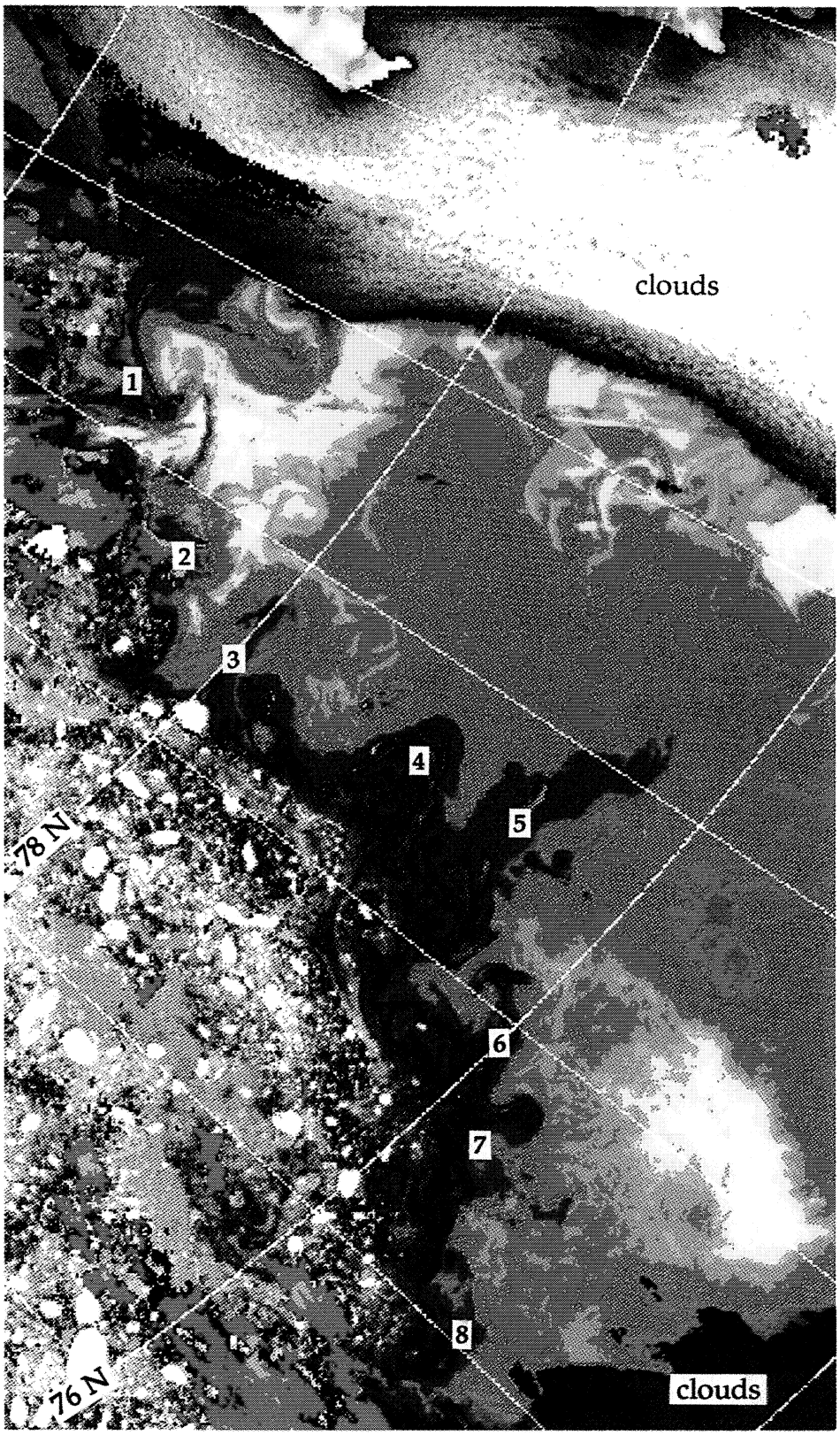

Plate 1. NOAA AVHRR image from July 1 1984 during the MIZEX 84 experiment. The image combined visual (channel 2) data over ice with IR data (channel 4) in open water. The dark blue indicates cold water along the ice edge, while light blue, red and yellow shows warmer water (> 2°C). The numbers indicate ice tongues similar to the SAR observations in MIZEX 87.

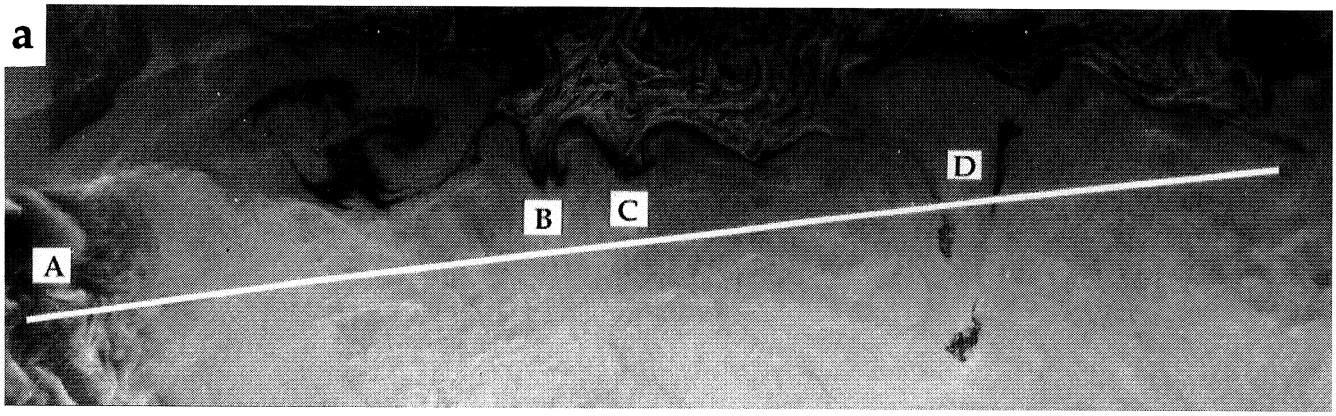
a
A
B
C
D

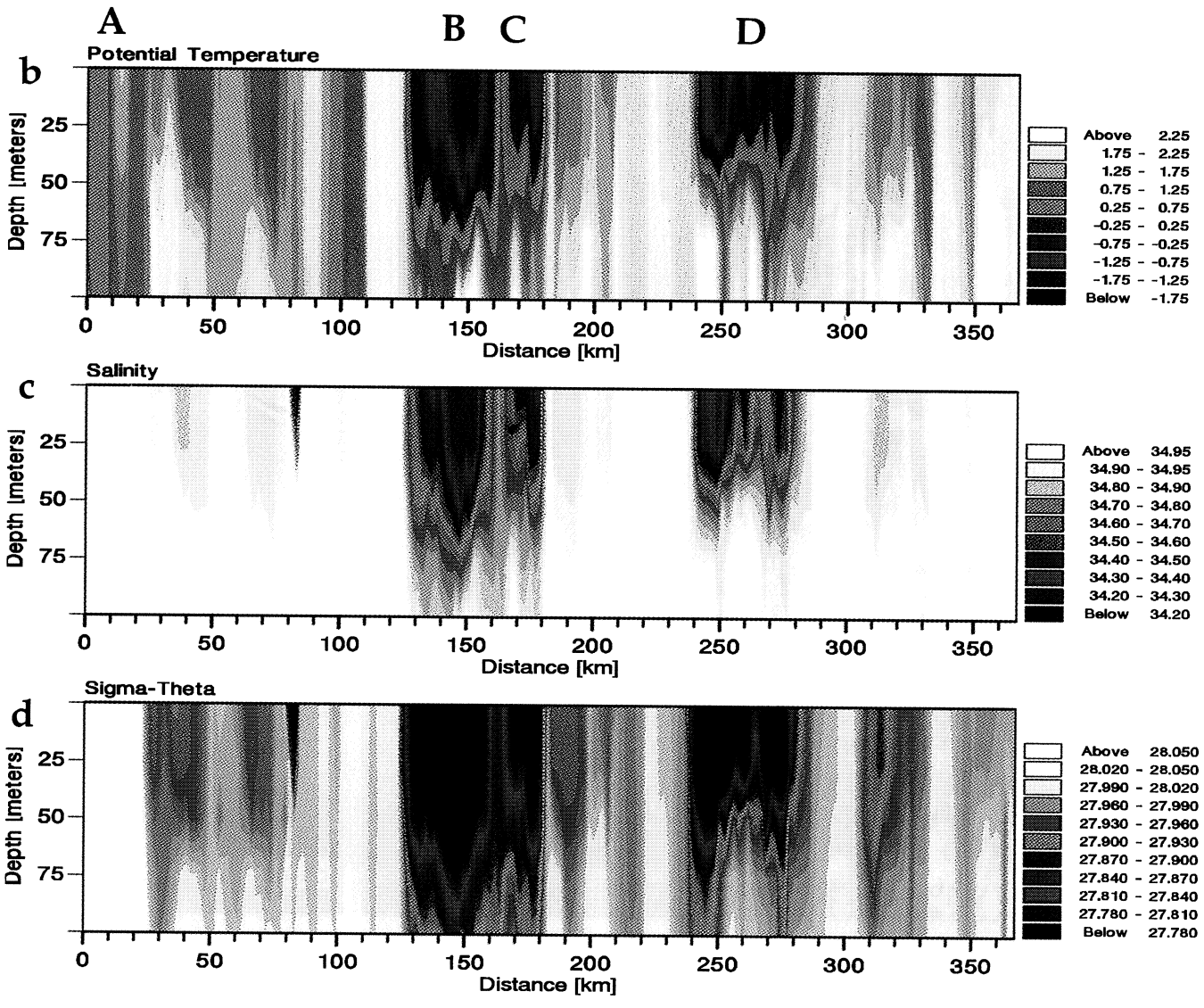
A
B C
D
b
Potential Temperature
Depth [meters]
25
50
75
0
50
100
150
200
250
300
350
Distance [km]
Above 2.25
1.75 - 2.25
1.25 - 1.75
0.75 - 1.25
0.25 - 0.75
-0.25 - 0.25
-0.75 - -0.25
-1.25 - -0.75
-1.75 - -1.25
Below -1.75
c
Salinity
Depth [meters]
25
50
75
0
50
100
150
200
250
300
350
Distance [km]
Above 34.95
34.90 - 34.95
34.80 - 34.90
34.70 - 34.80
34.60 - 34.70
34.50 - 34.60
34.40 - 34.50
34.30 - 34.40
34.20 - 34.30
Below 34.20
d
Sigma-Theta
Depth [meters]
25
50
75
0
50
100
150
200
250
300
350
Distance [km]
Above 28.050
28.020 - 28.050
27.990 - 28.020
27.960 - 27.990
27.930 - 27.960
27.900 - 27.930
27.870 - 27.900
27.840 - 27.870
27.810 - 27.840
27.780 - 27.810
Below 27.780

TABLE 1. List of symbols

$\mathbf{V}_i$	Transport in the ocean layer i
$\mathbf{v}_i$	Velocity in the ocean layer i
$\mathbf{f}$	$\mathbf{f} = f_0\mathbf{k}$, $f_0 = 1.427 \times 10^{-4}$ s^{-1}, Coriolis parameter
h_i	Thickness of ocean layer i
P_i	Pressure normalized by density in ocean layer i
	$P_i = g\eta - \delta_{i2}\, g'H_1$
A_{bh}	Biharmonic friction factor, $A_{bh} = 1 \times 10^7$ m^{4}s^{-1}
$\mathbf{X}$	Particle position
$\mathbf{v}_{1L}$	Lagrangian velocity in upper layer

be a valid approximation outside the main ice edge where the eddies and tongues were observed. However, further inside the ice edge internal ice stress must be invoked in realistic simulations.

3.2. Boundary and Initial Conditions

The model domain is a 128 by 108 km channel with periodic boundary conditions in the along-channel direction and no-slip side walls. The model schematization is as shown in Figure 17. The model bottom topography is a simplification of the East Greenland continental shelf break between 78° N and 79° N (we are not yet including the Greenland Fracture Zone). The topography is constant in the along-channel direction with flat-bottomed shelf and abyssal zones of depth 400 m and 2600 m, respectively. The two zones are connected by a slope of 0.11. The initial particle distribution is uniform over the ice covered area (the western half of the model area) with a density of 16 particles per km^2 for a total of over 54000 particles in a 27 km wide strip across the model domain. To simulate the core of the EGC the ocean is initialized with a Gaussian jet with a pressure field of the form

$$P_i = \left(\alpha_1 g\eta - \delta_{i2}\alpha_2 g' H_1\right)\exp\left(-\frac{y^2}{2L^2}\right) \qquad (3)$$

where α_1 and α_2 are constants defining the strength of the upper and lower layer jets, respectively, and L is the e-folding scale of the jet. The ocean velocity field is initially in geostrophic balance. The upper and lower layer jets are displaced from their axes with random perturbations. The jet displacements have an along-channel wavenumber spectrum of the form $\exp(-\beta\kappa)$, where $\beta = 5000/(2\pi)$ and κ is the wavenumber.

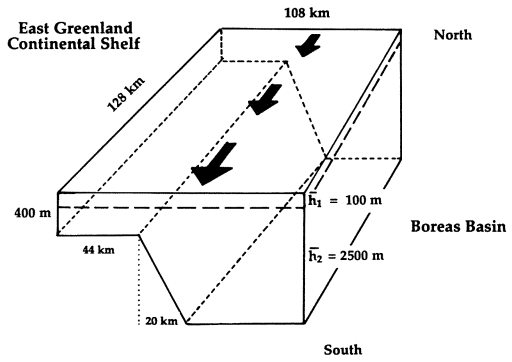

Fig. 17. Model schematization.

3.3. Numerical Scheme

A semi-implicit numerical scheme as described by *Hurlburt and Thompson* [1980] and *Smith and O'Brien* [1983] is used to perform the time integration of the primitive equations ocean model. An Arakawa "C" grid is used for the spatial discretization of the model. A time step of 300 s and a grid size of 1000 m between like variables are used in the study. The particle trajectories are computed by integrating the Lagrangian equation

$$\frac{d\mathbf{X}}{dt} = \mathbf{v}_{iL}(\mathbf{x}, \mathbf{t}) \qquad (4)$$

where $\mathbf{X}$ is the particle position and $\mathbf{v}_{iL}$ is the Lagrangian velocity, using a modified midpoint method [*Press et al.*, 1986] with four subintervals in each 300 s time step. Velocities were obtained through bilinear interpolation in space and linear interpolation in time.

4. NUMERICAL EXPERIMENTS

A series of numerical experiments were conducted with the eddy-resolving ocean model to examine the role of mixed barotropic/baroclinic instability in the formation of the observed ice edge eddies, tongues and vortex pairs described in section 2. The experiments are designed to determine the influence of jet width and intensity, topography and baroclinicity upon the generation and structure of the resulting ice tongues and vortex-pairs. The experiments conducted are summarized in Table 2. This series of experiments represents the first systematic study of ice tongues and vortex-pairs in the EGC.

Plate 2. (a) 100 km wide SAR image from the ERS-1 satellite obtained in January 1992 in the same area as MIZEX 87. The white line shows the location of a Seasoar section obtained by "Håkon Mosby" at the same time as the SAR image. Vertical structure of (b) temperature, (c) salinity and (d) density from the Seasoar section are shown in the upper 100 m.

TABLE 2. Summary of numerical experiments

Experiment number	Jet amplitude (m/s)	U_2/U_1	Topography	Jet width L (km)	H_1 (m)	H_2 (m)
1	0.4	0.33	yes	5	100	2500
2	0.4	0.33	no	5	100	2500
3	0.4	0	yes	5	100	2500
4	0.4	1	yes	5	100	2500
5	0.4	0.5	no	10	100	2500
6	0.4	0.5	yes	10	100	2500
7	0.4	0	no	5	100	2500
8	0.4	0.33	no	5	100	300

Case 1. Baseline Experiment

The baseline experiment consists of an upper layer jet representing the core of the EGC with amplitude 0.4 m/s situated over a lower layer jet with strength 0.13 m/s. Both jets flow from right to left (from north to south) in the along-channel direction centered over the shelf slope with shallower water on the right (Figure 17). The lateral e-folding scale, L, of both jets is 5 km for a total jet width of approximately 15 km. The upper layer mean thickness is 100 m, while the lower layer mean thickness is 2500 m. The reduced gravity parameter g', is 0.007 ms^{-2} with a resulting internal Rossby radius of deformation of approximately 5 km. These parameters were obtained from the observations described in section 2 and represented the marginal ice zone of the EGC north of about 77° N. The parameters are summarized in Table 2.

The results from the baseline experiment are depicted in Figure 18. In all panels the orientation is north on the right and south on the left. The contour interval for all sea level contour plots is 0.005 m. Negative sea level displacements are denoted by dashed contours. The displacement of the sea level provides a description of the circulation of the upper layer, since the upper layer pressure $p_1 = gh_1$ and the velocity field are nearly in geostrophic balance. By day 5 of the simulation undulations have appeared in the ice edge with a wavelength of 25 km. By day 7, the meanders have intensified and ice tongues have formed. The dominant wavelength has increased to about 32 km. By day 10, the ice tongues have evolved into 30 - 35 km long streamers. The series of graphs in Figure 18 shows how the jet instability process can serve to transport ice into open water. The change in orientation in the ice tongues is caused by shear in the jet, as discussed in section 2.2. The extents and growth rates of the tongues are summarized for each experiment in Table 3.

Case 2. Baseline Experiment with Flat Bottom.

To examine the role of the continental shelf, a simulation is performed with the same parameters as in Case 1 but with a flat bottom at a depth of 2600 m. By day 7 of this experiment, the velocity jet is broader than at the corresponding time in the baseline case where bottom topography was included (Figure 19). Furthermore, the excursions of the ice edge are larger, the ice tongues are broader and the displacements in the ice edge have longer wavelengths than in the baseline experiment. These results are consistent with the absence of the stabilizing effect of bottom slope and could therefore represent a situation where the ice edge is located further east over a flat deep bottom. In Case 1 the cross-isobath movement is suppressed somewhat by the presence of the shelf slope. In the experiment with a flat bottom the filaments are wider and the eddies are larger (30 - 40 km in diameter by day 7), but weaker compared to the baseline experiment.

Case 3. Baseline Experiment with Upper Layer Jet

In this experiment the ocean jet is initially constrained to exist only in the upper layer. Thus, the effects of enhanced baroclinicity can be examined. The stabilizing effect of the topography will also be lessened somewhat. After 9 days, the structure of the ice concentration (Figure 20) is similar to that of the baseline experiment except that the scale of the features has been reduced due to the enhanced baroclinicity. This experiment seems to be the most realistic of the 7 cases because the results are the most similar to the observations. The small vortex-pair evolving at the front of one of the ice filaments is similar to the observation in the SAR image in Figure 10 b. The distance between the simulated ice filaments is about 50 km. A vortex-pair which propagates into the ice (Figure 20 b) has a scale of about 30 km and resembles the vortex-pair seen in the SAR image in Figure 4 a, b. In the simulations it takes typically 5 days to build up instability which then creates tongues and vortex-pairs in 2 - 3 days. This is the same growth rate as was observed in the SAR images.

Case 4. Barotropic Jet

In the first experiment, conducted with a barotropic jet on a flat bottom, no development of instability occurred until

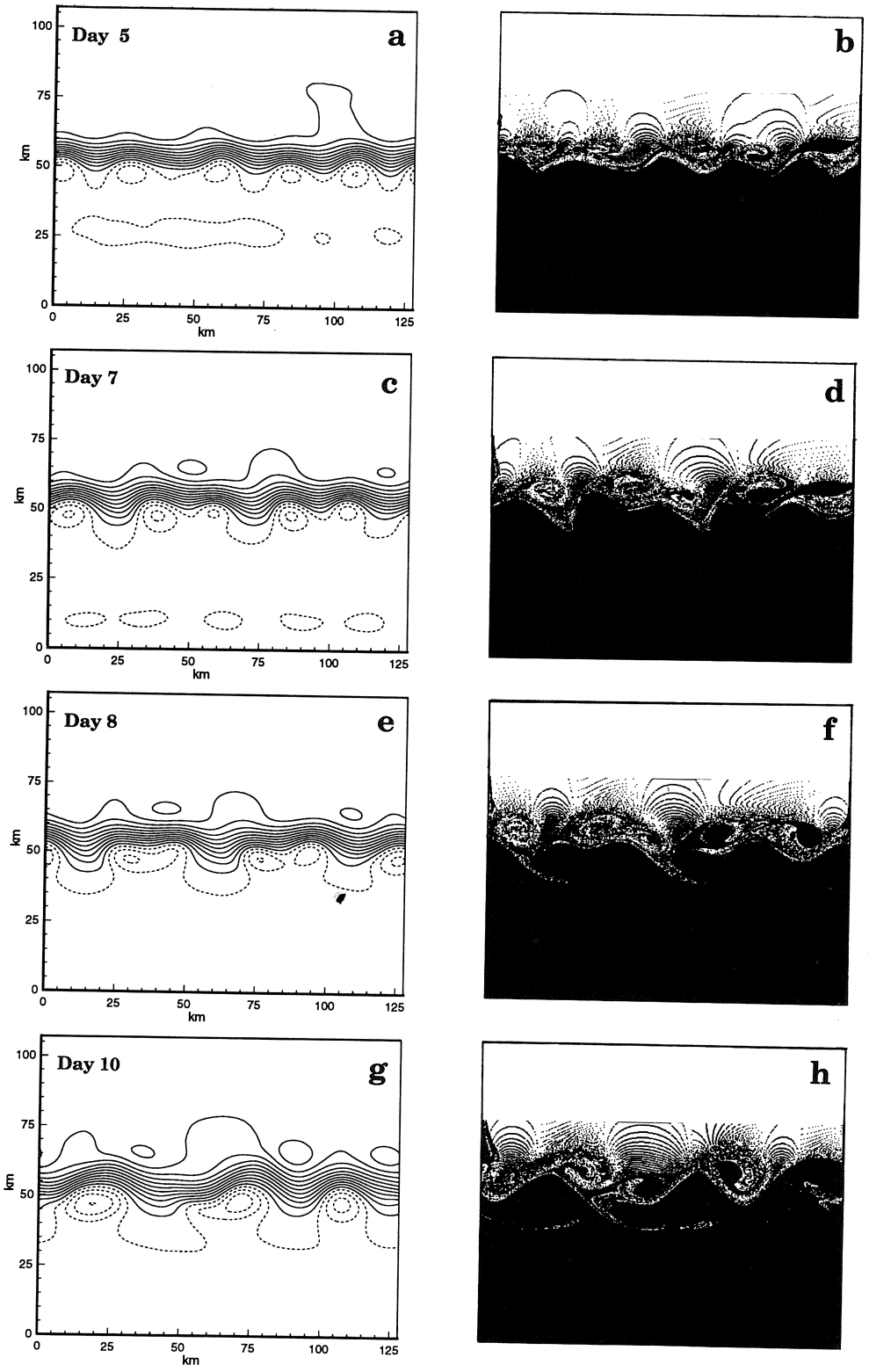

Fig. 18. Results from the Case 1 experiment after 5, 7, 8 and 10 days of simulations, (a, c, e, and g) surface height; (b, d, f, and h): corresponding particle distributions.

TABLE 3. Properties of computed ice filaments on day 9

Experiment number	Filament extent (km)	Growth rate (km/day)
1	33	15
2	26	7
3	33	11
4	49	14
5	20	6
7	29	30
8	60	10

after 18 days. By day 22, shown in Figure 21, the particle distribution developed a large sinusoidal meander pattern with a wavelength of about 40 km. The regular sinusoidal particle distribution is not representative of the typical ice patterns observed by the SAR images. In the second experiment, where shelf slope topography was included, a stable jet was produced. No instability developed after 40 days of simulation. The second experiment is a more realistic simulation of the EGC flowing along the shelf break and suggests that the core of the EGC is not necessarily unstable.

Case 5. Broader Baroclinic Jet with Flat Bottom

In this case there is a flat bottom, the lower layer jet velocity amplitude is increased to 0.2 m/s, the upper layer

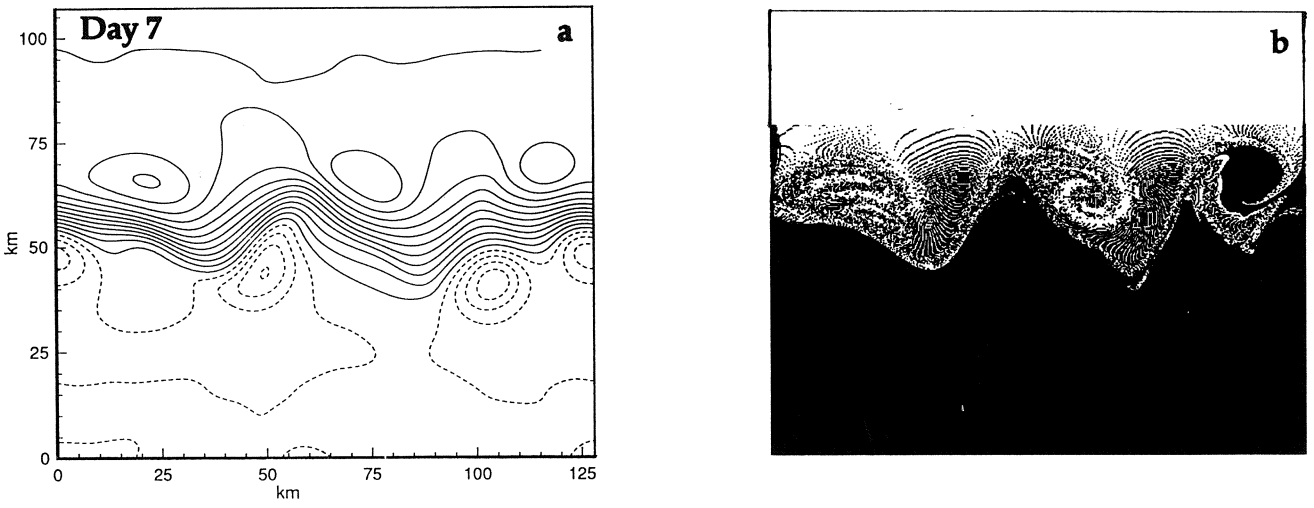

Fig. 19. Results from the Case 2 experiment after 7 days. (a) Surface height and (b) particle distribution.

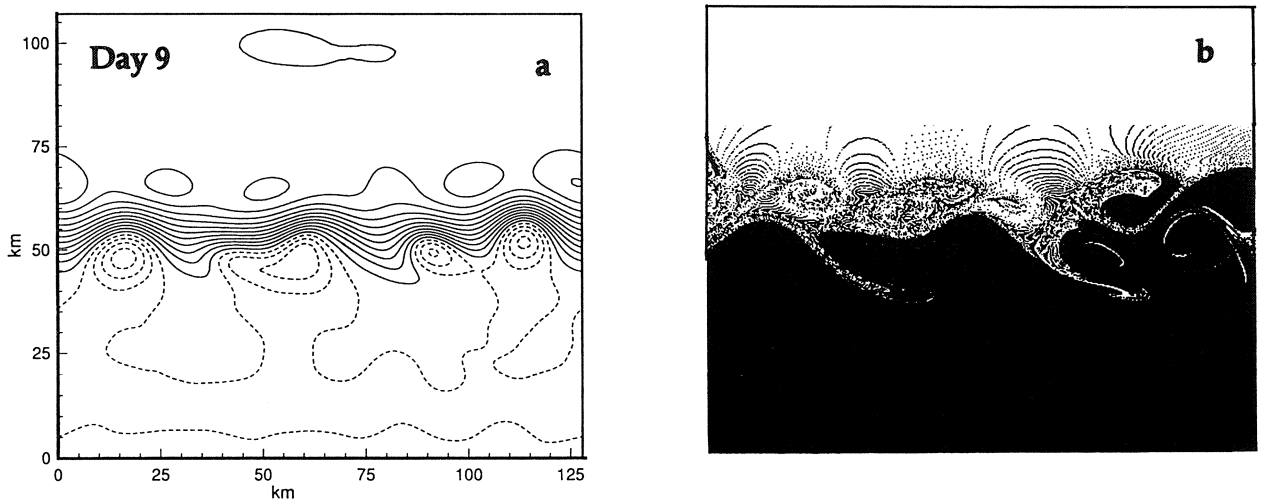

Fig. 20. Results from the Case 3 experiment after 9 days. (a) Surface height and (b) particle distribution.

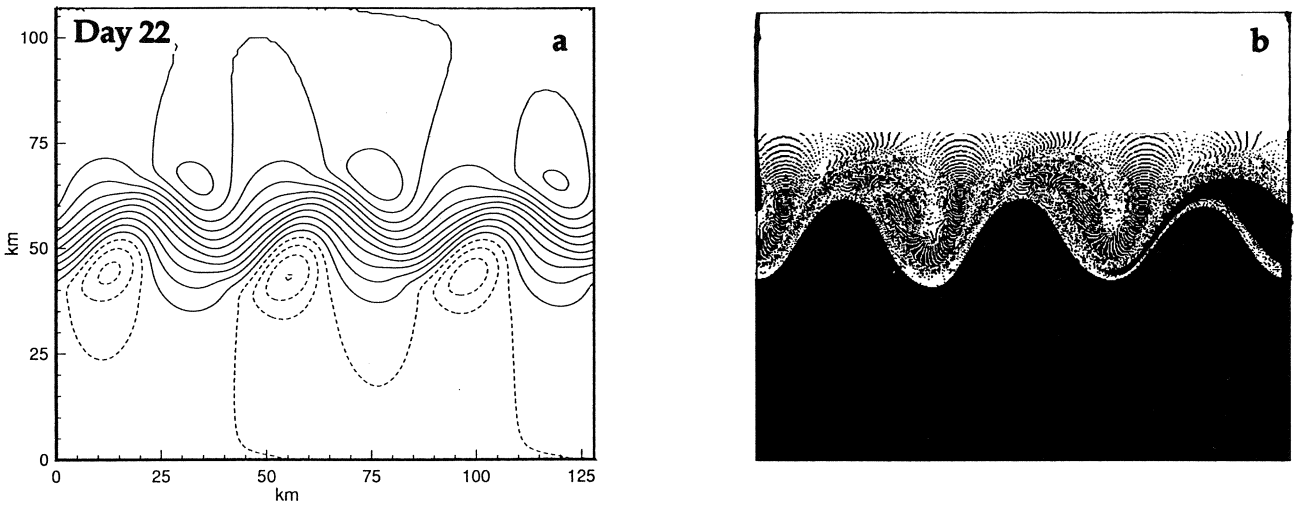

Fig. 21. Results from the Case 4 experiment after 22 days. (a) Surface height and (b) particle distribution.

amplitude remains at 0.40 m/s, and the jet width scale, L, is increased to 10 km. The growth rate for this case is less than half that of the baseline case. Two ice tongues associated with anticyclonic eddies of diameter 30 - 40 km have evolved separated by 60 - 70 km (Figure 22). Larger scale disturbances evolve in this experiment than in the previous cases.

Case 6. Broad Baroclinic Jet with Topography

This case is similar to the baseline experiment but with a wider jet and increased lower layer velocity. When shelf slope topography is included, there is no instability even after 30 days. The topography again stabilizes the jet. This case may be most representative of typical conditions when the EGC flows as a stable jet locked to the shelf break.

Case 7. Upper Layer jet with Flat Bottom

This experiment is similar to Case 3 but with a flat bottom at a depth of 2600 m. It represents the case where an intense upper layer jet is advected into deep water. From Figure 23 it can be seen that the characteristic length scale is somewhat larger than in Case 3. The instability in this case is initially stronger. This is due to the absence of the stabilizing effect of the bottom topography. After 6 days the instability has slowed to a very low growth rate.

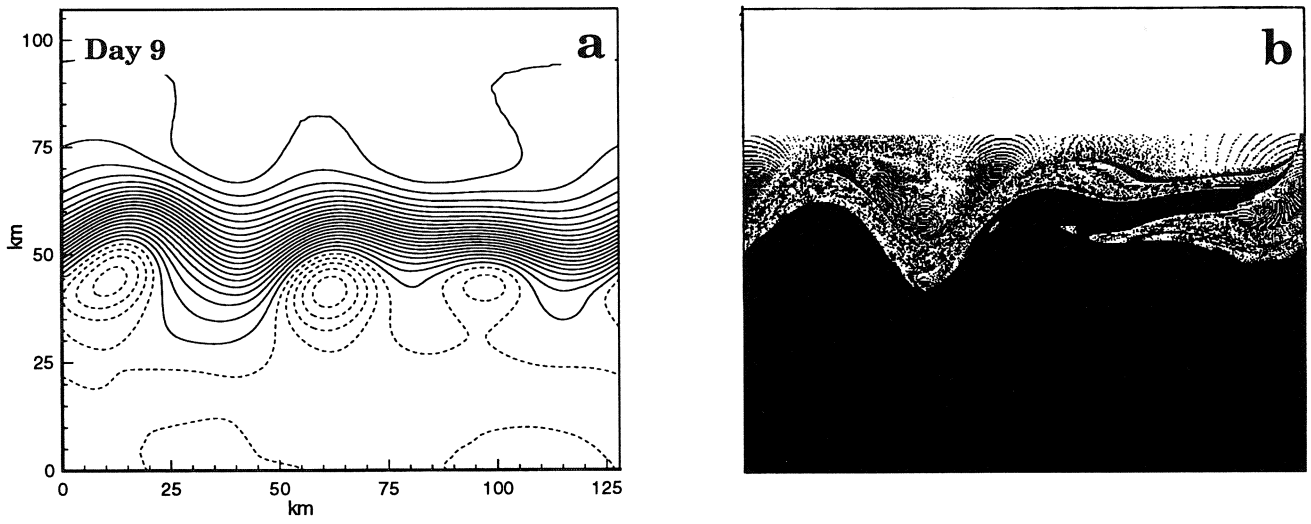

Fig. 22. Results from the Case 5 experiment after 9 days. (a) Surface height and (b) particle distribution.

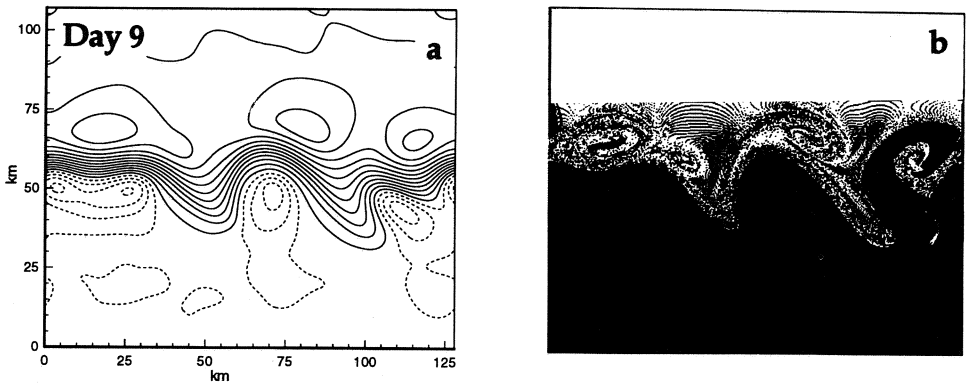

Fig. 23. Results from the Case 7 experiment after 9 days. (a) Surface height and (b) particle distribution.

Case 8. Baseline Experiment with Flat Shelf Topography

In this experiment there is a flat bottom at a depth of 400 m. This case simulates the response of an ice edge jet over the continental shelf. This experiment is similar to Case 2, but with a shallower depth. From Figure 24 it can be seen that the instability is more energetic than in Case 1 and 2.

4.2. DIAGNOSTIC ANALYSES

For a more quantitative description of the model simulation results, linear stability analyses and power spectral analyses were performed on the model output for selected experiments.

The linear stability analysis is based upon a two-layer quasi-geostrophic model. The analysis method is that of *Holland and Haidvogel* [1980], with the exception that the topographic-beta term has been included to model the effects of the bottom topography. The results of the analyses are the wavelength and e-folding scale of the growth rate of the most unstable wave. At days 0, 3, 6 and 9 the mean cross-channel profiles are computed from the model output and used in the stability analysis.

Shown in Table 4 are the linear stability results for cases 1, 2, 3, 5, 7, and 8, which are the key experiments in this study. It can be seen that the general tendency is for the wavelength of the most unstable mode and the e-folding time of the growth rate to increase over time. This is due to the jet-eddy interactions producing a broadening and weakening of the jet. The effect of eddy dynamics is to stabilize the system over time. It should be noted that several unstable modes are present in the system at any given time. Different modes will be the fastest growing at various times. Thus, in Case 8, for example, a mode with a shorter wavelength becomes dominant at day 9. The e-folding times of 1 - 3 days during days 3 - 6 for the most realistic cases, 1 and 3, are consistent with the field observations of the evolution of the ice tongues. The characteristic wavelengths of 28 - 38 km for these cases from Table 4, corresponding to eddy diameters of 14 - 19

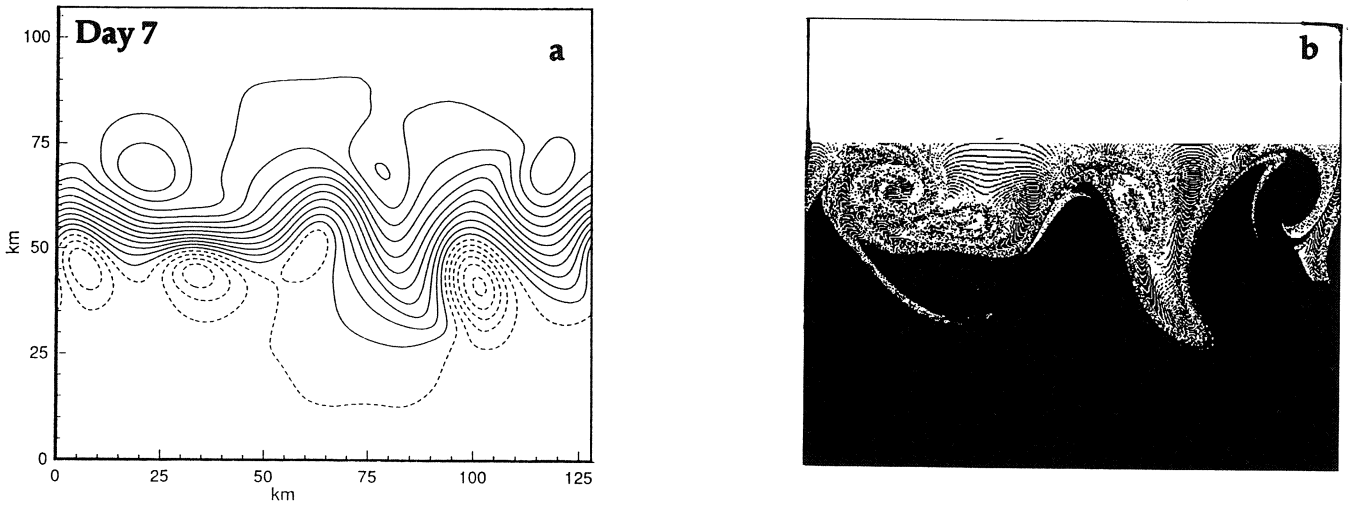

Fig. 24. Results from the Case 8 experiment after 7 days. (a) Surface height and (b) particle distribution.

TABLE 4. Linear stability analysis results

Experiment number	Wavelength (km)				E-folding time (days)			
	Day 0	Day 3	Day 6	Day 9	Day 0	Day 3	Day 6	Day 9
1	21	30	38	48	0.56	1.1	2.2	3.0
2	21	34	49	56	0.56	1.6	4.5	6.1
3	19	28	38	38	0.55	1.1	3.1	3.6
5	41	55	61	76	1.60	2.2	2.6	3.8
7	19	32	50	86	0.55	1.7	6.8	11.8
8	21	36	70	45	0.56	1.8	4.9	4.1

km, are within the observed range of eddy scales in the marginal ice zone of the Greenland Sea.

To obtain estimates of the dominant zonal length scales produced in the model simulations, a maximum entropy spectral analysis [*Press et al.*, 1986] was performed on the model results. The analysis was based on 30 coefficients and computed for a 10 km wide, along-channel strip which was centered over the initial jet position. The results were checked for consistency against periodograms computed from Fast Fourier Transforms. The results from the analysis are illustrated in Figure 25 a, b where the kinetic energy (KE) spectral density is plotted against wavelength for Case 1 and 3. The evolution of the KE spectrum over the course of the simulations is depicted in the graphs. In both cases the KE distribution is bimodal, with peaks at 24 - 26 km and 42 - 45 km. Initially, the peak at wavelength 24 - 26 km builds up rapidly, reaching its maximum at day 5 in Case 1 and day 7 in Case 3, but as time progresses energy is transferred to the 42 - 45 km scale. From Figure 18 and 20, these results can be interpreted as eddy events, where the eddies have typical diameters of 12 - 13 km and are separated by 42 - 45 km.

Cases 2 and 5 also exhibit a second clear spectral peak at a larger wavelength, at 44 - 51 km and 53 - 55 km, respectively. The low wavenumber portion of the spectra from Cases 7 and 8 varied too much over time to permit a simple characterization of a larger length scale.

These results are summarized in Table 5. Also shown in this table are the growth rates for the velocity amplitudes at the dominant scales. These values are compared to the growth rates determined from the linear stability analysis (LSA) at the same wavelengths.

A comparison of Tables 4 and 5 is instructive. Scale 1 in Table 5, which corresponds to twice a typical eddy diameter, is consistently smaller than the wavelength of the most unstable mode predicted from the LSA for day 3, as shown in Table 4. The model Scale 2 values for Case 1 and 3, which have topography, are larger than the LSA-predicted values at day 6. However, the model Scale 2 values for the non-topography Case 2 and 5 are longer than

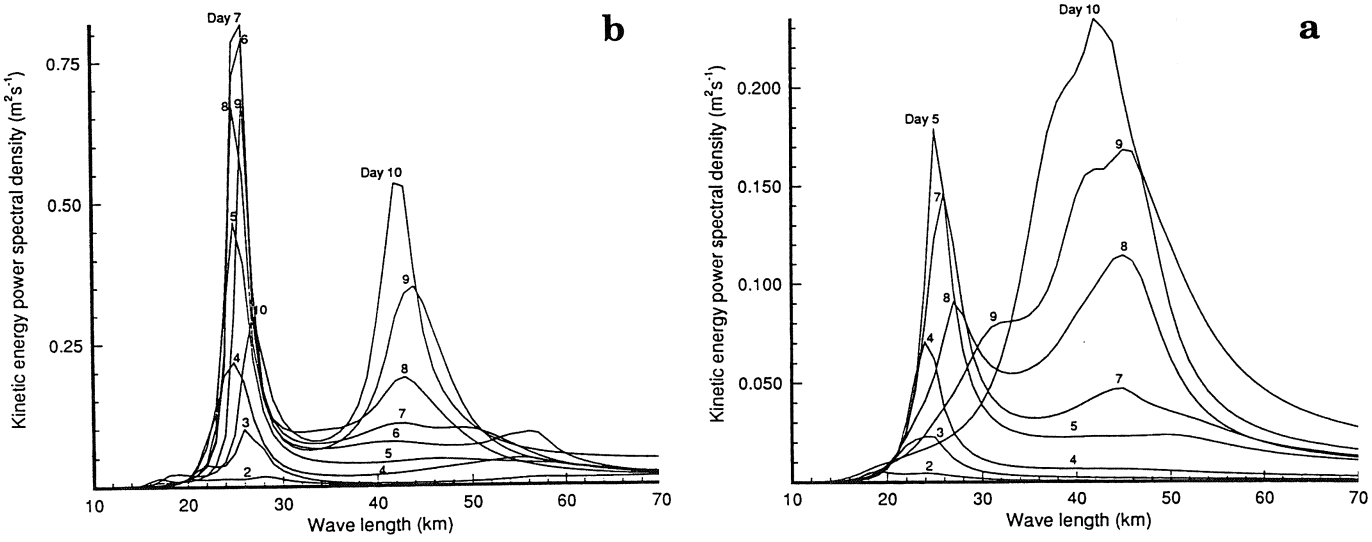

Fig. 25. Kinetic Energy Spectra for different days in (a) Case 1 and (2) Case 3.

TABLE 5. Dominant length scales and associated growth rates

Case	Scale (km)	Growth rate ($x10^{-6}s^{-1}$)	LSA growth rate ($x10^{-6}s^{-1}$)
	Scale 1		
1	24 - 25	5.7	6.1
2	34 - 35	2.0	4.0
3	25 - 26	4.4	6.7
5	33 - 35	3.0	0.5
7	27 - 30	1.4	3.1
8	29 - 32	6.6	6.1
	Scale 2		
1	42 - 45	3.7	3.6
2	44 - 51	1.2	2.8
3	41 - 44	3.4	3.3
5	53 - 55	2.7	9.8

those of the day 6 LSA. These differences in the larger dominant length scales may be partially attributable to the differences in the representation of bottom topography in the two-layer primitive equation and the quasigeostrophic models.

The model and LSA growth rates are in good agreement for cases 1, 3 and 8. The e-folding growth rate time scales of 2.0 days for Case 1 and 2.6 days for Case 3 for the eddy-containing 24 - 26 km length scale are consistent with the field observations discussed in section 2.

5. DISCUSSION

Ice tongues and vortex pairs are most readily observed along the ice edge where the images show a sharp contrast between ice and water. Vortex-pairs may also occur within the ice and in the open ocean, but here they are more difficult to detect in the SAR images as well as in other remote sensing data. But do they also occur frequently elsewhere in the ocean? What physical conditions are necessary to generate ice tongues and vortex pairs and what is their characteristic temporal and spatial distribution? Based on a large number of observations, *Fedorov and Ginsburg* [1986] argue that filaments with attached vortex pairs occur frequently in the ocean. The problem is to observe them systematically. So far only remote sensing data and simulation experiments have been able to catch the phenomenon, and then only in cases where a tracer is present.

The evolution of two counter-rotating vortices can be considered to be a consequence of the conservation of the initial angular momentum of the jet. This has been demonstrated in a series of laboratory experiments in which a variety of modes of forcing were applied to a rotating fluid [*Flierl et al.*, 1983]. The underlying generating mechanisms are frontal instabilities associated both with the ice edge and the ocean front which are present in the area. Such instabilities can produce all sorts of meanders, tongues and eddies. However, it is not clear whether vortex-pairs are just random manifestations of the turbulent eddy field, or if they are caused by specific mechanisms, as shown in this study. Another possibility is that the structures can be produced by the action of an impulsive surface stress as shown by *Mied et al.* [1991] for the open ocean.

A series of numerical experiments was carried out to examine the sensitivity of the evolution of ice edge eddies, tongues and vortex pairs to variations in model parameters. A general result from all the experiments is that although the ice distribution fields evolve into complicated structures within a few days, the velocity fields remain relatively simple with the along-channel jet slightly perturbed by weak eddies. Meanders in the velocity field are sufficient to generate off-ice tongues and filaments similar to the observations described in section 2.1 and 2.2. One must be careful to avoid confusing a Lagrangian tracer distribution with an instantaneous Eulerian circulation pattern.

An encouraging aspect of the numerical investigation has been that the spatial structure of the observed ice filaments and vortex pairs is very similar to the computed fields in Case 1 (Figure 18) and Case 3 (Figure 20). In these cases the most realistic parameter settings were used.

In a comparison of the observed and modelled ice jet evolution, summarized in Table 3, it is seen that the modelled ice tongue growth rate and extent in Case 1 and 3 corresponds well to the observed values. Furthermore, the structure of the sea ice is also similar to the observations in the SAR images.

In order to assess the significance of the instability processes on the transport of sea ice in the Greenland Sea, lateral flux calculations using particle distributions were conducted. The number of particles positioned seaward (away from the ice edge) from the initial ice edge (center of the jet) after 10 days was tabulated for each of the simulations in cases 1, 3, 5, 7, and 8. If each particle is assumed to cover a surface area of 250 x 250 m, with ice concentration of 0.8 and thickness of 1 m [*Shuchman et al.*, 1994], it is possible to compute an ice volume flux associated with eddy activity. The ice mass flux is estimated by examining the transport of particles seaward averaged over a two - day period of the most intense eddy activity. It is assumed that these conditions are representative of the marginal ice zone for 150 days per year. The seaward ice flux extrapolated from the 128 km long model domain for the 2000 km extent of the MIZ is given in Table 6.

If it is assumed that each of the particles (ice floes) advected seaward melts, then the Case 1 and 3 estimates of

TABLE 6. Seaward ice flux between 76° and 80°N

Experiment number	Ice mass flux (km^3/year)
1	273
2	109
3	120
5	121
7	264
8	442

273 and 120 $km^3 year^{-1}$ respectively, correspond to an ice edge melt rate of 0.9 and 0.4 km per day. These values are comparable to the estimates based on direct melt observations by *Johannessen et al.* [1987] for eddy-induced ice edge melt of 1 - 2 km per day.

The melt rate caused by eddies can also be estimated directly by assuming that ice edge eddies are present 150 days of the year along 2000 km of the EGC. This eddy melting mechanism of 1 km per day in 150 days will cause an annual melt of 300 km^3 assuming an ice thickness of 1 m. This estimate is in agreement with the results from the model simulations presented in Table 6. It is approximately 12 % of the annual transport of 2600 km^3 per year past 79° N [*Kvambekk and Vinje*, 1993], implying that the ice edge eddies are important and should be included in regional modelling of the ice edge location. This "eddy-melt" process will also contribute to the freshwater budget of the Greenland Sea, causing increased stabilization of the surface layer and reduced winter convection.

Wind forcing was not applied in the simulations since the wind conditions during the MIZEX 87 experiment were moderate to light and the main driving mechanism on the ice motion was the ocean circulation. When the wind is above 12 - 15 m/s, the ice is mainly driven by the wind forcing and the surface signature of the ocean circulation is masked. Under such conditons the SAR images cannot be used to study the mesoscale ocean features. In the most pronounced wind events observed during the MIZEX 87 experiment (10 - 12 m/s) the wind acted in the opposite direction of the ice tongues and was therefore not considered to be the driving force for these tongues.

Acknowledgements. This study has been supported by Office of Naval Research, University of Bergen and Environmental Research Institute of Michigan. Computing for this study was conducted at the IBM Bergen Environmental Services and Solutions Centre. Special thanks go to the SAR aircraft crews from INTERA Technologies Ltd., and to the crews onboard R/V "Polar Circle" and R/V "Håkon Mosby" for excellent cooperation in the field experiment.

REFERENCES

Couder, Y. and C. Basdevant, Experimental and numerical study of vortex couples in two-dimensional flows, *J. Fluid Mech, 173*, 225-251, 1986.

Fedorov, K. N. and A. I. Ginsburg, "Mushroom-like" currents (vortex dipoles) in the ocean and in a laboratory tank, *Annales Geophysicae, 4,* B, 5, 507-515, 1986.

Fedorov, K. N. and A. I. Ginsburg, Mushroom-like currents (vortex dipoles): One of the most widespread forms of non-stationary coherent motions in the ocean, in *Mesoscale/Synoptic Coherent Structures in Geophysical Turbulence*, edited by J. C. J. Nihoul and B. M. Jamart, pp. 1-14, 1989.

Flierl, G. R., M. E. Stern, and J. A. Whitehead, The physical significance of modons: laboratory experiments and general integral constraints, *Dyn. of Atmos. and Oceans, 7,* 233-263, 1983.

Holland and Haidvogel, A parameter study of the mixed instability of ideal ocean currents. *Dyn. Atmos. Oceans, 4,* 185 - 215, 1980.

Hurlburt, H. E. and J. D. Thompson, A numerical study of Loop Current intrusions and eddy shedding, *J. Phys. Oceanogr., 9,* 1611-1651, 1980.

Johannessen, O. M., J. A. Johannessen, J. Morison, B. A. Farrelly and E. A. S. Svendsen, Oceanographic conditions in the marginal ice zone north of Svalbard in early fall 1979 with an emphasis on mesoscale processes. *J. Geophys. Res., 88,* 2755-2769, 1983.

Johannessen, O. M., J. A. Johannessen, E. Svendsen, R. A. Shuchman, W. J. Campbell, and E. Josbergeer, Ice-edge eddies in the Fram Strait Marginal Ice Zone. *Science, 236,* 427-729, 1987a.

Johannessen, J. A., O. M. Johannessen, E. Svendsen, R. Shuchman, T. Manley, W. J. Campbell, E. G. Josberger, S. Sandven, J. C. Gascard, T. Olaussen, K. Davidson, and J. Van Leer, Mesoscale eddies in the Fram Strait marginal ice zone during 1983 and 1984 Marginal Ice Zone Experiments, *J. Geophys. Res., 97,* 6754-6772, 1987b.

Johannessen, O. M., W. J. Campbell, R. Shuchman, S. Sandven, P. Gloersen, J. A. Johannessen, E. G. Josberger, and P. M. Haugan. Microwave study programs of air-ice-ocean interactive processes in the seasonal ice zone of the Greenland and Barents seas, in *Microwave Remote Sensing of Sea Ice* Geophys. Monogr. Ser., vol. 68, edited by F. Carsey, pp. 261 - 289, AGU, Washington, 1992.

Kvambekk, Å. S., and T. Vinje, The ice transport through the Fram Strait. (abstract) Nansen Centennial Symposium, June 21 - 25, Nansen Environmental and Remote Sensing Center, 1993.

Mied, R. P., J. C. McWilliams and G. J. Lindemann. The generation and evolution of Mushroom-like Vortices. *J. Phys. Ocean.ogr 21*, 489 - 510, 1991.

MIZEX Group, MIZEX East 83/84: The summer Marginal Ice Zone Program in the Fram Strait/Greenland Sea. *EOS, Trans. AGU 67,* No.23, 513-517, 1986.

MIZEX Group, MIZEX East 1987: The winter Marginal Ice Zone Program in the Fram Strait/Greenland Sea. *EOS, Trans. AGU 70,* No.17, 545, 1989.

Narimousa, S., and T. Maxworthy, Coastal upwelling on a sloping bottom: the formation of plumes, jets and pinched-off cyclones, *J. Fluid Mech. 176,* 169-190, 1987.

Press, W. H., B. P. Flannery, S. A. Tekolsky, and W. T. Vetting, *Numerical Recipes. The Art of Scientific Computing,* 818 pp., Cambridge, University Press, Cambridge, 1986.

Quadfasel, D., and J. Meincke, Note on the thermal structure of the Greenland Sea. *Deep Sea Res., 34,* 1883-1888, 1987.

Røed, L. P., and J. J. O'Brien, A coupled ice-ocean model of upwelling in the marginal ice zone, *J. Geophys. Res., 88,* 2863-2872, 1983.

Shuchman, R. A., C. L. Rufenach, and O. M. Johannessen, The extraction of marginal ice zone thickness using gravity wave imagery. *J. Geophys. Res.* (in press) 1994.

Smith, D. C. IV, and J. J. O'Brien, The interaction of a two-layer isolated mesoscale eddy with topography, *J. Phys. Oceanogr., 13,* 1681-1697, 1983.

Smith, D. C. IV, and A. A. Bird, The interaction of an ocean eddy with an ice edge ocean jet in a marginal ice zone, *J. Geophys. Res., 96,* 4675-4690, 1991.

O. M. Johannessen, S. Sandven, W. P. Budgell, J. A. Johannessen, NERSC, Edv. Griegsvei 3a, N-5037 Solheimsvik, Norway.

R. A. Shuchman, ERIM, P. O. Box 134001, Ann Arbor, MI 48113-4001.